Human-level reinforcement learning performance of recurrent neural networks is linked to hyperperseveration, not directed exploration

D. Tuzsus[1], I. Pappas[2], J. Peters[1]

[1]Department of Psychology, Biological Psychology, University of Cologne, Germany

[2]Department of Neurology, Keck School of Medicine, University of Southern California, USA

Contact:

Author contributions:

Conceptualization: DT, IP, JP. Methods: DT, IP, JP. Implementation: DT, IP. Writing (first draft): DT. Writing (review and editing): JP, IP. Supervision: JP. Funding acquisition: JP.

Acknowledgements:

This work was funded by Deutsche Forschungsgemeinschaft (PE1627/8-1, Code 496990750 to J.P.).

Abstract

A key feature of animal and human decision-making is to balance exploring unknown options for information gain (directed exploration) versus exploiting known options for immediate reward, which is often examined using restless bandit problems. Recurrent neural network models (RNNs) have recently gained traction in both human and systems neuroscience work on reinforcement learning. Here we comprehensively compared the performance of a range of RNN architectures as well as human learners on restless four-armed bandit problems. The best-performing architecture (LSTM network with computation noise) exhibited human-level performance. Cognitive modeling showed that human and RNN behavior is best described by a learning model with terms accounting for perseveration and directed exploration. However, whereas human learners exhibited a positive effect of uncertainty on choice probability (directed exploration), RNNs showed the reverse effect (uncertainty aversion), in conjunction

with increased perseveration. RNN hidden unit dynamics revealed that exploratory choices were associated with a disruption of choice predictive signals during states of low state value, resembling a win-stay-loose-shift strategy, and resonating with previous single unit recording findings in monkey prefrontal cortex. During exploration trials, RNN selected exploration targets predominantly based on their recent value, but tended to avoid more uncertain options. Our results highlight both similarities and differences between exploration behavior as it emerges in RNNs, and computational mechanisms identified in cognitive and systems neuroscience work.

Introduction

Reinforcement learning (RL) theory (Sutton & Barto) is of central importance in psychology, neuroscience, computational psychiatry and artificial intelligence as it accounts for how artificial and biological agents learn from reward and punishment. According to both the law of effect in psychology (Thorndike, 1927) and the reward hypothesis in machine learning (Sutton & Barto, 2018), agents optimize behavior to maximize reward and minimize punishment. In computational psychiatry, RL theory has yielded valuable insights into changes in learning and decision-making associated with different mental disorders (Huys et al., 2016; Maia & Frank, 2011; Yahata et al., 2017).

To maximize reward, agents have to solve the exploration-exploitation dilemma (Sutton & Barto, 2018) that can be stated as follows: Should one pursue actions that led to reward in the past (exploitation) or should one explore novel courses of action for information gain (exploration)? In stable environments, where rewards corresponding to actions are fixed across time, the exploration-exploitation dilemma can be effectively solved by first exploring all available actions to identify the most rewarding one, and subsequently exploiting this action. In contrast, in volatile environments, rewards corresponding to actions change across time, such that exploration and exploitation need to be continuously balanced by an agent. A high level of exploitation would make an agent unable to adapt to changes in the environment, whereas too much exploration would reduce reward accumulation, as optimal actions would oftentimes not be selected.

A number of computational strategies have been proposed to address the exploration-exploitation tradeoff (Sutton & Barto, 2018). In ε-greedy and softmax choice rules, exploration is achieved via choice randomization. While such “random” exploration appears to be one core component of both human and animal exploration (Daw et al., 2006; Ebitz et al., 2018; Schulz & Gershman, 2019; Wilson et al., 2014, 2021), computational modeling of behaviour strongly suggests that humans additionally use “directed” or strategic exploration strategies (Chakroun

et al., 2020; Schulz & Gershman, 2019; Speekenbrink & Konstantinidis, 2015; Wiehler et al., 2021; Wilson et al., 2014, 2021). This is typically modeled via an “exploration bonus” parameter that increases the value of options with greater information value (Chakroun et al., 2020; Speekenbrink & Konstantinidis, 2015; Wiehler et al., 2021; Wu et al., 2018). In volatile environments, the uncertainty associated with the outcome of a specific action is often taken as a proxy for information gain (Wilson et al., 2021). Exploring uncertain courses of action can thus increase information gain, over and above a simpler random exploration strategy.

In humans, exploratory choices are associated with increased activity in the fronto-parietal network (Beharelle et al., 2015; Chakroun et al., 2020; Daw et al., 2006; Wiehler et al., 2021) and regulated by dopamine and norepinephrine neuromodulatory systems (Chakroun et al., 2020; McClure et al., 2005; Swanson et al., 2020). Choice predictive signals in prefrontal cortex neural populations are disrupted during exploratory choices, reflecting a potential neural mechanism for random exploration (Ebitz et al., 2018).

Such neuroscientific lines of work have increasingly been informed by computational neuroscience approaches (Mante et al., 2013). Here, artificial neural network models are applied to shed light on the computational principles underlying task performance. In the context of reinforcement learning problems, recurrent neural network models (RNNs) are particularly powerful tools. They constitute deep artificial neural network models for sequential data (LeCun et al., 2015) and can be trained to solve RL problems using training signals derived from RL theory (Botvinick et al., 2020). Agents interact with the environment, and receive environmental feedback (e.g., rewards) based on their actions, which then informs subsequent choices. RNNs can be applied to such learning problems due to their recurrent connectivity pattern. Each time step, RNN hidden units receive information regarding the network’s activation state at the previous time step via these recurrent connections, thereby equipping the network with memory about what has happened before. Training and analysis of such models offer potential novel insights with implications for neuroscience (Botvinick et al., 2020). For example, the representations that emerge in a network’s hidden unit activation pattern following training (or over the course of training) can be directly analyzed (Findling & Wyart, 2020; Mante et al., 2013; Tsuda et al., 2020; Wang et al., 2018), similar to the analysis of high-dimensional neural data (Cunningham & Yu, 2014; Ebitz et al., 2018; Mante et al., 2013). This can reveal insights into the computations and representations underlying a network’s performance.

Neural network modeling approaches also complement computational modeling as typically done in psychology and cognitive neuroscience (Farrell & Lewandowsky, 2018). In this classical approach, computational mechanisms and representations hypothesized to underlie performance of a given task are explicitly and rigidly build into a quantitative model. While this approach is helpful to compare candidate models, the rigid dependency of these

models on built-in a priori assumptions preclude the discovery of novel mechanisms and representations that could underlie task performance. In contrast, RNN dynamics and representations might reveal novel potential mechanisms and representations that support similar tasks by virtue of the RNNs independent data-driven learning capacity (Botvinick et al., 2020). Reward learning (Findling & Wyart, 2020; Tsuda et al., 2020; Wang et al., 2018) and decision-making (Findling & Wyart, 2020; Mante et al., 2013) are prominent recent examples.

To this end, RNNs have recently been successfully trained on reinforcement learning and decision-making tasks from the human and animal neuroscience literature (Findling & Wyart, 2021; Mante et al., 2013; Song et al., 2017; Tsuda et al., 2020; Wang et al., 2018). Such networks achieved a form of “meta-learning”, where eventhough weights were held fixed following extensive training, the models had acquired the capability to solve novel instantiations of tasks from the same task family (Dasgupta et al., 2019; Findling & Wyart, 2021; Tsuda et al., 2020; Wang et al., 2018). In meta-learning, reinforcement learning operating over a large number of training episodes via slow adjustments of network weights, gave rise to a much faster reinforcement learning algorithm embedded in the network dynamics, and not involving further weight changes (Botvinick et al., 2020; Findling & Wyart, 2021; Wang et al., 2018). Finally, evidence suggests that RNNs with noisy computations might be more resilient to adverse conditions (e.g. contingency reversals, volatility) than their counterparts with deterministic computations (Findling & Wyart, 2020). This resonates with findings from the machine learning literature suggesting improved performance of neural networks with noisy computations under some conditions (Dong et al., 2020; Fortunato et al., 2019; Qin & Vucinic, 2018). Likewise, mental representations (Drugowitsch et al., 2016) and neural representations (Findling et al., 2019; Findling & Wyart, 2021; Renart & Machens, 2014) might benefit from some degree of representational imprecision (e.g., representations infused with task-independent noise). Thus, RNNs trained on multiple instantiations from a task family (meta-learning) and equipped with noisy computations are potentially excellent candidates to solve cognitive tasks.

Allowing RNNs to learn on cognitive tasks and comparing their behavior to human agents is a promising endeavour. However, it should be noted that RNNs can diverge from human behaviour in terms of strategy deployed or tasks that they can solve. RNNs might show human-like behavior by mere statistical learning without the use of human-like abstract rule learning (Kumar et al., 2022). Also, while deep RL agents show superhuman ability in games like Go, Shogi, Chess and Atari games (Mnih et al., 2015; Silver et al., 2017, 2018) they fail to perform better than an agent with random action selection on a standard T-maze task from animal learning (Wauthier et al., 2021). In the artificial intelligence and machine learning literature, one of the most prominent differences between human and artificial agents is the number of interactions with the environment required to learn the task (Botvinick et al., 2019;

Lake et al., 2015; Marcus, 2018; Tsividis et al., 2021). This is in part related to exploration inefficiency ("sampling inefficiency") with respect to collecting sufficient informative experiences during training (Hao et al., 2023). Even though there is ongoing work on endowing deep RL agents with improved exploration strategies (Hao et al., 2023; Ladosz et al., 2022; Tsividis et al., 2021), direct comparisons to human agents suggests differences. For example, Binz & Schulz (2022) showed that the large state-of-the-art artificial neural network model GPT-3 shows no evidence of directed exploration in a modified bandit task ("Horizon Task"), were reward and information are decorrelated (Wilson et al., 2014). Taken together, artificial agents can show exceptional problem-solving capabilities, but still diverge from human-level intelligence under some circumstances, especially in how exploration is used to guide learning.

Bandit tasks constitute a classical testing bed for RL agents (Sutton & Barto, 2018), and are regularly applied to study human and animal exploration (Beharelle et al., 2015; Chakroun et al., 2020; Daw et al., 2006; Ebitz et al., 2018; Findling et al., 2019, 2019; Hamid et al., 2016; Mohebi et al., 2019; Wiehler et al., 2021). In non-stationary (*restless*) bandit tasks, agents select among a number of options ("bandits") with dynamically changing reinforcement rates or magnitudes (Fig. 1 b & c). In contrast, in stationary bandit problems reinforcement rates are fixed. RNNs achieve state-of-the-art performance on stationary bandit tasks (Wang et al., 2018) and adapt to volatility in reversal schedules (Behrens et al., 2007; Wang et al., 2018). Furthermore, RNNs with computation noise can solve restless bandit tasks when trained on stationary bandits (Findling & Wyart, 2020), in contrast to their counterparts with deterministic computations. Human exploration behavior in restless bandit tasks is typically better accounted for by models with dynamic uncertainty-dependent learning rates such as the Kalman Filter (Daw et al., 2006; Kalman, 1960). Furthermore, humans regularly apply a directed exploration strategy on restless bandit tasks. This is modeled using an additional "exploration bonus" parameter that typically takes on positive values, reflecting directed exploration of uncertain options (Beharelle et al., 2015; Chakroun et al., 2020; Speekenbrink & Konstantinidis, 2015; Wiehler et al., 2021; Wilson et al., 2021; Wu et al., 2018).

Initial work on RNN mechanisms supporting bandit task performance (Findling & Wyart, 2020; Song et al., 2017; Wang et al., 2018), have predominantly focused on stationary bandits (Wang et al., 2018). However, stationary bandits preclude a comprehensive analysis of exploration mechanisms, because exploration behavior is restricted to the first few trials. Furthermore, previous work often focused on two-armed bandit problems (Findling et al., 2019; Findling & Wyart, 2020; Song et al., 2017). However, these tasks are limited in that only one alternative can be explored at any given point in time. Although previous work has begun to use classical computational modeling to better understand RNN behavior (Fintz et al., 2022; Wang et al., 2018), a comprehensive comparison of human and RNN behavior and

computational mechanisms when solving the exact same RL problems is still lacking. In addition, similar to so-called researcher's degrees of freedom in experimental work (Wicherts et al., 2016), the study of RNNs is associated with a large number of design choices, e.g. with respect to the specifics of the architecture, details of the training schemes as well as hyperparameter settings. Yet, a comprehensive comparison of different network architectures and design choices in the context of RL tasks from the human cognitive neuroscience literature is still lacking. Here, we addressed these issues in the following ways. First, we comprehensively compared a large set of RNN architectures in terms of their ability to exhibit human-level performance on restless four-armed bandit problems. Second, to compare computational strategies between RNNs and human subjects, we used comprehensive cognitive modeling for both human and RNN behavior during performance of the exact same RL problems. Finally, we expanded upon previous approaches to the analysis of RNN hidden unit activity patterns (Findling & Wyart, 2020; Mante et al., 2013; Wang et al., 2018) by applying dimensionality reduction techniques previously applied in the study of primate exploration behavior (Ebitz et al., 2018).

Methods

RNN unit types

The present study systematically compared network architectures consisting of four different types of RNN units, standard recurrent units ("vanilla" units) (Elman, 1990), standard LSTM units (Hochreiter et al. 1997), as well as both unit types endowed with computation noise.

Vanilla RNN

This is a simple Elman recurrent neural network (Elman, 1990) ("Vanilla" RNN). Let X_t denote the input to the network at time t, H_t the recurrent state of the network and Y_t the output of the network. Then the network is governed by the following equations:

$$\widehat{H}_{\mathrm{t}} = W_{H_{t-1}} \cdot H_{t-1} + W_X \cdot X_t + B \tag{1}$$

$$H_t = \sigma_{tanh}(\widehat{H}_t) \tag{2}$$

$$Y_t = \sigma_{sm}(W_H \cdot H_t) \tag{3}$$

The input X_t is a vector of length 5 with the first element corresponding to the reward observed on the previous trial (r_{t-1}) and the remaining elements containing a one-hot encoding of the previously chosen action (a_{t-1}). The latter is a vector of length 4 (No. of actions) with all elements being "0" except the element which corresponds to the previous action being set to

"1". The parameters of the network are weight matrices $W_{H_{t-1}}$, W_X and W_H and the bias vector B, which are optimized during the training process. Non-linear activation functions σ_{tanh} and σ_{sm} denote the hyperbolic tangent and the softmax function, respectively.

The forward pass of the model starts by passing information from the input layer to the hidden layer by calculating the updated state $\widehat{H_t}$ as a linear combination of the input X_t and the previous recurrent activity H_{t-1} weighed by corresponding weight matrices W_X and $W_{H_{t-1}}$ and an additive bias term B (Eq. 1). Within the hidden layer, $\widehat{H}_t$ is non-linearly transformed by the hyperbolic tangent function which results in the current recurrent activity H_t (Eq. 2). Recurrent activity H_t in the hidden layer is then transformed to action probabilities Y_t by applying the softmax function to H_t weighed by matrix W_H (Eq. 3).

Noisy Vanilla RNN

Computation noise might aid in adverse conditions during decision-making (Findling & Wyart, 2020). Following Findling et al. (2020), we therefore modified the standard RNN unit by adding update-dependent computation noise to the recurrent activity H_t.

$$\widehat{H}_{t,k}^{noisy} \sim \mathcal{N}\left(\widehat{H}_{t,k}, \zeta \cdot \left|H_{t-1,k}^{noisy} - H_{t,k}\right|\right) \tag{4}$$

To transform the exact recurrent activity $H_{t,k}$ in unit k in trial t to noisy recurrent activity $H_{t,k}^{noisy}$ we added noise according to a Gaussian distribution with mean equal to the exact updated state $\widehat{H}_{t,k}$ (see Eq. 1) and a standard deviation of the absolute magnitude of the difference between the previous noisy recurrent activity $H_{t-1,k}^{noisy}$ and the current exact recurrent activity $H_{t,k}$ (see Eq. 2). Because of this difference term the spread of the noise added to a unit scales with the amount of reconfiguration in recurrent activity between subsequent trials similar to a prediction error. The standard deviation is further scaled by the hyperparameter $\zeta > 0$ denoted the *Weber fraction* (Findling & Wyart, 2020). Finally, after having sampled the noisy updated state $\widehat{H}_{t,k}^{noisy}$ the hyperbolic tangent activation function is applied (see Eq. 2) to calculate noisy recurrent activity $H_{t,k}^{noisy}$. Importantly, similar to Findling et al. (2020) we treated computation noise as an endogenous constraint to the network were the source of the noise is not modifiable, thereby ignoring the gradients resulting from it in the optimization procedure during gradient descent.

LSTM

One issue with standard vanilla RNN units is that during gradient descent, they can suffer from exploding and vanishing gradient problems, resulting in the network not learning the task (Rehmer & Kroll, 2020). Long short-term memory networks (LSTMs) solve this problem by using gated units that control the information flow, which allows the network to learn more long term dependencies within the data (Hochreiter & Schmidhuber, 1997).

LSTM behaviour is governed by the following standard equations:

$$I_{\mathrm{t}} = \sigma_{sm}(W_{XI} \cdot \mathrm{X}_t + W_{HI} \cdot \mathrm{H}_{t-1} + W_{CI} \cdot C_{t-1} + B_I) \tag{5}$$

$$F_{\mathrm{t}} = \sigma_{sm}(\mathrm{W}_{XF} \cdot \mathrm{X}_{\mathrm{t}} + \mathrm{W}_{\mathrm{HF}} \cdot H_{\mathrm{t}-1} + \mathrm{W}_{\mathrm{CF}} \cdot C_{\mathrm{t}-1} + B_F) \tag{6}$$

$$C_t = F_t \circ C_{\mathrm{t}-1} + I_t \circ \sigma_{tanh}(W_{XC} \cdot \mathrm{X}_{\mathrm{t}} + W_{HC} \cdot H_{t-1} + B_C) \tag{7}$$

$$O_t = \sigma_{sm}(W_{XO} \cdot \mathrm{X}_{\mathrm{t}} + W_{HO} \cdot H_{t-1} + W_{CO} \cdot \mathrm{C} + B_O) \tag{8}$$

$$H_t = O_t \circ \sigma_{tanh}(C_t) \tag{9}$$

Here, X is the same input as in Vanilla RNNs, I is the input gate, F is the forget gate (also called the maintenance gate), C is the cell state, O is the output gate, H is the hidden state, t indexes trials and σ_{sm} and σ_{tanh} denote the softmax or the hyperbolic tangent activation function, respectively. The trainable parameters of the network are weight matrices W and the bias vectors B, where subscripts indicate the connected gates/states.

Noisy LSTM

Following Findling & Wyart (2020), we introduce Weber noise at the level of the hidden state H of an LSTM unit k at trial t:

$$H_{t,k}^{noisy} \sim \mathcal{N}\left(H_{t,k}, \zeta \cdot \left|H_{t-1,k}^{noisy} - H_{t,k}\right|\right) \tag{10}$$

That is, noisy LSTM units are the direct analogue to the noise extension outlined above for vanilla units.

Training and test environments

Networks were trained and tested on four-armed restless bandit tasks (Daw et al., 2006). On each trial, agents choose between one of four actions (bandits). Associated rewards slowly drift according to independent gaussian random walks. A single episode during training and testing consisted of 300 trials.

During training, the reward associated with the ith bandit on trial t was the reward on trial t-1, plus noise:

$$\hat{R}_{i,t} = R_{i,t-1} + \epsilon_{i,t} \tag{11}$$

Noise ϵ was drawn from a gaussian distribution with mean 0 and standard deviation 0.1:

$$\epsilon_{\mathrm{i,t}} \sim \mathcal{N}(0,\ 0.1) \tag{12}$$

To ensure a reward range of [0,100], reflecting boundaries were applied such that

$$\mathrm{R_{i,t}} = \begin{cases} R_{i,t-1} + \epsilon_{i,t} & if\ 0 < \hat{R}_{i,t} < 100 \\ R_{i,t-1} - \epsilon_{i,t} & if\ \hat{R}_{i,t} < 0\ or\ \hat{R}_{i,t} > 100 \end{cases} \tag{13}$$

Following training, networks weights were fixed, and performance was examined on three random walk instances previously applied in human work (Chakroun et al., 2020; Daw et al., 2006; Wiehler et al., 2021). Here, the reward associated with the i_{th} bandit on trial t was drawn from a gaussian distribution with standard deviation 4 and mean $\mu_{i,t}$ and rounded to the nearest integer.

$$R_{i,t} \sim \mathcal{N}\left(\mu_{i,t}, 4\right) \tag{14}$$

On each trial, the means diffused according to a decaying gaussian random walk:

$$\mu_{i,t+1} = \lambda\mu_{i,t} + (1-\lambda)\theta + \epsilon_{\mathrm{i,t}} \tag{15}$$

with decay $\lambda = 0.9836$ and decay center $\theta = 50$. The diffusion noise $\epsilon_{\mathrm{i,t}}$ was sampled from a gaussian distribution with mean 0 and SD 2.8:

$$\epsilon_{\mathrm{i,t}} \sim \mathcal{N}(0,\ 2.8) \tag{16}$$

Each network was exposed to the same three instantiations of this process used on human work (Chakroun et al., 2020; Daw et al., 2006; Wiehler et al., 2021).

Training procedure

The networks were trained to optimize their weights and biases by completing 50.000 task episodes. For each episode, a new instantiation of the environment was created according to the equations above. We compared two training schemes, the standard REINFORCE algorithm (Williams & Peng, 1991) and advantage actor-critic (A2C, Mnih et al., 2016). The objective of the network was to maximize the expected sum of discounted rewards according to following equation:

$$\mathrm{L}(\pi) = \mathrm{E}^{\pi}\left[\sum_{t\geqq 1}\sum_{k\geqq 0}\gamma^{k}\cdot r_{t+k}\right] \tag{17}$$

Here, t is the trial number, γ the discount factor, t_{t+k} the observed reward at trial $t+k$ (k is a positive integer) and π is the policy followed by the network.

Following each episode, one of the following algorithms was used to update the network parameters to improve the policy. REINFORCE (Williams & Peng, 1991) relies on a direct differentiation of the objective function:

$$\nabla \mathrm{L}_{\pi} = E^{\pi}\left[\sum_{t\geqq 1}\nabla l\,og\pi(a_t)\cdot\left(\sum_{k\geqq 0}\gamma^{k}\cdot r_{t+k}\right)\right] \tag{18}$$

Here the gradient of the policy loss ($\nabla \mathrm{L}_{\pi}$) is calculated by summing the derivatives of the log probabilities of chosen actions ($log\pi(a_t)$) weighted by the discounted sum of expected rewards from the current trial until the end of the episode. Note that this ensures that action probabilities will increase or decrease according to the expected rewards following these actions. If the expected returns $\left(\sum_{k\geqq 0}\gamma^{k}\cdot r_{t+k}\right)$ are positive, the gradient will be positive and therefore gradient descent will increase the log probabilities of chosen actions. Conversely, if expected returns are negative, the gradient will be negative and therefore gradient descent will decrease the log probabilities of chosen actions. Thus, action probabilities for actions that led to rewards will be increased, and action probabilities for actions that led to punishments will be decreased.

Advantage Actor-Critic (A2C, Mnih et al., 2016) uses a weighted sum of the policy gradient (∇L_{π}), the gradient with respect to the state-value function loss (∇L_{v}), and an optional entropy regularization term (∇L_{ent}), defined as follows:

$$\nabla L = \nabla L_{\pi} + \nabla L_{v} + \nabla L_{ent} \tag{19}$$

$$= \frac{\partial \log \pi(a_t|\theta)}{\partial \theta} \delta_t(\theta) + \beta_v \delta_t(\theta) \frac{\partial V}{\partial \theta_v} + \beta_e \left[\frac{\partial H\big(\pi(a_t|\theta)\big)}{\partial \theta} \right]$$

$$\delta_t(\theta_v) = [G_t - V(\theta_v)] \tag{20}$$

$$G_t = \sum_{i=0}^{k} \left[\gamma^i r_{t+1} + \gamma^k V(\theta_v) \right] \tag{21}$$

Here, on a given trial t, the chosen action is denoted by a_t, the discounted return is G_t with k being the number of steps until the end of the episode, the actor component with the action policy π is parameterized by RNN parameters θ, the critic component with the value function V estimating the expected return is parameterized by θ_v, the entropy of policy π is denoted by $H(\pi)$, the advantage function that estimates the temporal-difference error is denoted by $\delta_t(\theta_v)$. A2C in this formulation contains two hyperparameters β_v and β_e scaling the relative influence of the state-value function loss and the entropy regularization term, respectively.

Note that in equations 19 – 21, RNN parameters corresponding to the policy θ and to the value function θ_v are seperated, but in practice, as in Wang et al. (2018), they share all layers except the output layer where the policy corresponds to a softmax output and the value function to a single linear output. Weights and biases for REINFORCE and A2C were updated using the RMSProp algorithm as implemented in Tensorflow 1.15.0.

A common problem of policy gradient methods such as REINFORCE is high variance in the gradients used during the stochastic gradient descent (SDG) optimization procedure (Sutton & Barto, 2018). This is the case because the magnitude of the gradients depends on the empirical returns (sum of collected rewards in a given episode). We therefore mean-centered rewards to reduce the variance in the gradients, which improved the training process and performance.

A subset of hyperparameters were systematically varied, as outlined in Table 1. The entropy cost (β_e) was either set to 0.05 (fixed entropy), linearly annealed over the course of training from 1 to 0, or omitted (*none*). In networks with computation noise, the Weber fraction ζ was set to 0.5 (Findling et al., 2020). Additional hyperparameters (learning rate, discount factor, no. of training episodes etc.), were selected based on previous work (Wang et al., 2018) and held constant across all architectures (see Table 2).

Table 1. Overview of factors that are systematically explored in RNN training. Total number of RNN models: 2 (Unit type) x 2 (Computation noise) x 3 (Entropy cost) x 2 (Learning algorithm) = 24 RNN models.

Factor

Unit type	Vanilla / LSTM
Computation noise	None / Update-dependent
Entropy cost β_e	None / Fixed / Annealed
Learning algorithm	REINFORCE / A2C

Table 2. Hyperparameter values used during RNN training.

Hyperparameters	
Number of hidden units	48
Learning rate	0.0001
State-value estimate cost β_v	0.5
Weber fraction ζ	0.5
Discount factor	0.5
Training Episodes	50.000
Trials per Episode	300

Human data

For comparison with RNN behavior, we re-analyzed human data from a previous study (placebo condition of Chakroun et al. (2020), n=31 male participants). Participants performed 300 trials of the four-armed restless bandit task as described in the environment section.

Cognitive modeling

Our model space for RNN and human behavior consisted of a total of 14 models (see Table 3). Each model consisted of two components, a *learning rule* (Delta rule or Bayesian learner) describing value updating, and a *choice rule* mapping learned values onto choice probabilities.

Delta rule: Here, agents update the expected value (v_{c_t}) of the bandit chosen on trial t (c_t) based on the prediction error (δ) experienced on trial t:

$$v_{c_t,t+1} = v_{c_t,t} + \alpha\delta_t \tag{22}$$

$$\delta_t = R_t - v_{c_t,t} \tag{23}$$

The learning rate $0 \leq \alpha \leq 1$ controls the fraction of the prediction error used for updating, and R_t corresponds to the reward obtained on trial t. Unchosen bandit values are not updated between trials and thus remain unchanged until a bandit is chosen again. Bandit values were initialized at $v_1 = 50$.

Bayesian learner: Here we used a standard Kalman filter model (Daw et al., 2006; Kalman, 1960), where the basic assumption is that agents utilize an explicit representation of the process underlying the task's reward structure. The payoff in trial t for bandit i follows a decaying Gaussian random walk with mean $\mu_{i,t}$ and observation variance $\theta_o^2 = 4^2$. Payoff expectations ($\hat{\mu}_{i,t}^{pre}$) and uncertainties (variances $\hat{\sigma}_{i,t}^{2\,pre}$) for all bandits are updated between trials according to

$$\hat{\mu}_{i,t+1}^{pre} = \hat{\lambda}\hat{\mu}_{i,t}^{post} + \left(1 - \hat{\lambda}\right)\hat{\vartheta} \tag{24}$$

and

$$\hat{\sigma}_{i,t+1}^{2\,pre} = \hat{\lambda}^2\hat{\sigma}_{i,t}^{2\,post} + \hat{\sigma}_d^2 \tag{25}$$

with decay $\lambda = 0.9836$, decay center $\vartheta = 50$ and diffusion variance $\hat{\sigma}_d^2 = 4$.
The chosen bandit's mean is additionally updated according to

$$\hat{\mu}_{c_t,t}^{post} = \hat{\mu}_{c_t,t}^{pre} + \kappa_t\delta_t \tag{26}$$

with

$$\delta_t = r_t - \hat{\mu}_{c_t,t}^{pre}. \tag{27}$$

Here, κ denotes the Kalman gain that is computed for each trial t as:

$$\kappa_t = \hat{\sigma}_{i,t}^{2\,pre}/\left(\hat{\sigma}_{i,t}^{2\,pre} + \hat{\sigma}_o^2\right) \tag{28}$$

κ_t determines the fraction of the prediction error that is used for updating. In contrast to the learning rate in the delta rule model, $\kappa_t$varies from trial to trial, such that the degree of updating scales with a bandit's uncertainty $\hat{\sigma}_{i,t}^{2\,pre}$. The observation variance $\hat{\sigma}_o^2$ indicates how much rewards vary around the mean, reflecting how reliable each observation is for estimating the true mean. Initial values $\mu_1^{pre}$and $\sigma_1^{2\,pre}$ were fixed to 50 and 4 for all bandits, respectively.

Estimates of the random walk parameters $\hat{\lambda}$, $\hat{\vartheta}$, $\hat{\sigma}_o^2$ and $\hat{\sigma}_d^2$ were fixed to their true values (see Table 3).

Choice rules: delta rule models

Choice rule 1 used a standard softmax function (SM):

$$\text{Choice rule 1 (SM)}: \; P_{i,t} = \frac{exp(\beta v_{i,t})}{\sum_j e\,xp(\beta v_{j,t})} \tag{29}$$

Here, $P_{i,t}$ denotes the probability of choosing bandit i on trial t and β denotes the inverse temperature parameter controlling the degree of choice stochasticity.

Choice rule 2 extended choice rule 1 with a heuristic directed exploration term:

$$\text{Choice rule 2 (SM + T)}: \; P_{i,t} = \frac{exp(\beta[v_{i,t} + \varphi(t - T_i)])}{\sum_j e\,xp(\beta[v_{j,t} + \; \varphi(t - T_j)])} \tag{30}$$

This simple "trial heuristic" (Speekenbrink & Konstantinidis, 2015) models a bandit's uncertainty as linearly increasing with the number of trials since it was last selected $(t - T_i)$, where T_i denotes the last trial before the current trial t in which bandit i was chosen. The free parameter φ models the impact of directed exploration on choice probabilities.

Choice rule 3 then replaced the trial-heuristic with a directed exploration term based on a "bandit identity" heuristic:

$$\text{Choice rule 3 } (SM + B): P_{i,t} = \frac{exp(\beta[v_{i,t} + \varphi x_i])}{\sum_j \mathrm{e\,xp}(\beta[\mathrm{v_{j,t}} + \varphi \mathrm{x_j}])} \tag{31}$$

Here, x_i denotes how many unique bandits were sampled since bandit i was last sampled. E.g., $x_i = 0$ if bandit *i* was chosen on the last trial, and $x_i = 1$ if one other unique bandit was selected since *i* was last sampled. x_i therefore ranges between 0 and 3.

Choice rule 4 then corresponds to choice rule 1 with an additional first-order perseveration term:

$$\text{Choice rule 4 (SM + P)}: \mathrm{P_{i,t}} = \frac{\exp(\beta[v_{i,t} + I_{c_{t-1=i}}\rho])}{\sum_j \exp\left(\beta\left[\mathrm{v_{j,t}} + \mathrm{I_{c_{t-1=j}}}\rho\right]\right)} \tag{32}$$

The free parameter ρ models a perseveration bonus for the bandit selected on the preceding trial. I is an indicator function that equals 1 for the bandit chosen on trial $t-1$ and 0 for the remaining bandits.

Choice rules 5 and 6 likewise extend choice rules 3 and 4 with perseveration terms:

$$Choice\ rule\ 5\ (SM+TP):\ P_{i,t} = \frac{exp\left(\beta\left[v_{i,t} + \varphi(t-T_i) + I_{c_{t-1=i}}\rho\right]\right)}{\sum_j exp\left(\beta\left[v_{j,t} + \varphi(t-T_j) + I_{c_{t-1=j}}\rho\right]\right)} \tag{33}$$

$$Choice\ rule\ 6\ (SM+BP): P_{i,t} = \frac{exp\left(\beta\left[v_{i,t} + \varphi x_i + I_{c_{t-1=i}}\rho\right]\right)}{\sum_j exp\left(\beta\left[v_{j,t} + \varphi x_j + I_{c_{t-1=i}}\rho\right]\right)} \tag{34}$$

Choice rules: Bayesian learner models

with $\hat{\mu}_{i,t}^{pre}$ instead of $v_{i,t}$ in Equations 29, 30, 31, 32, 33 and 34 yields choice rules 1-6 for the Kalman filter models (equations omitted for brevity). Given that the Bayesian Learner models include an explicit representation of uncertainty, we included two additional models:

$$Choice\ rule\ 7\ (SM+E): P_{i,t} = \frac{exp\left(\beta\left[\hat{\mu}_{i,t}^{pre} + \varphi\hat{\sigma}_{i,t}^{pre}\right]\right)}{\sum_j \exp\left(\beta\left[\hat{\mu}_{j,t}^{pre} + \varphi\,\hat{\sigma}_{j,t}^{pre}\right]\right)} \tag{35}$$

Here, φ denotes the exploration bonus parameter reflecting the degree to which choice probabilities are influenced by the uncertainty associated with each bandit, based on the model-based uncertainty $\hat{\sigma}_{i,t}^{pre}$. Again including first order perseveration yields choice rule 8:

$$Choice\ rule\ 8\ (SM+EP): P_{i,t} = \frac{exp\left(\beta\left[\hat{\mu}_{i,t}^{pre} + \varphi\hat{\sigma}_{i,t}^{pre} + I_{c_{t-1=i}}\rho\right]\right)}{\sum_j \exp\left(\beta\left[\hat{\mu}_{j,t}^{pre} + \varphi\,\hat{\sigma}_{j,t}^{pre} + I_{c_{t-1=j}}\rho\right]\right)} \tag{36}$$

Table 3. Free and fixed parameters of all computational models.

Note: Choice rules for the Delta rule: Choice rule 1: softmax; Choice rule 2: softmax with directed exploration (trial heuristic); Choice rule 3: softmax with directed exploration (bandit heuristic); Choice rule 4: softmax with perseveration; Choice rule 5 and 6 are choice rules 2 and 3 with perseveration. Choice rules for the Bayes learner rule: Choice rule 1: softmax; Choice rule 2: softmax with directed exploration (Kalman-Filter); Choice rule 3: softmax with directed exploration (trial heuristic); Choice rule 4: softmax with directed exploration (bandit heuristic); Choice rule 5: softmax with perseveration; Choice rules 6 – 8 are choice rules 2-

4 with perseveration; α: learning rate; β: inverse temperature; φ: exploration bonus; ρ: perseveration bonus; v_1: initial expected reward values for all bandits; λ: decay parameter; $\hat{\vartheta}$: decay center; σ_o^2: observation variance; σ_d^2: diffusion variance; μ_1^{pre}: initial mean of prior expected rewards for all bandits; σ_1^{pre}:initial standard deviation of prior expected rewards for all bandits.

	Delta rule		**Bayesian learner**	
Choice rule 1	α, β	Fixed: v_1	β	Fixed: $\hat{\lambda}$, $\hat{\vartheta}$, $\hat{\sigma}_o^2$, $\hat{\sigma}_d^2$, $\hat{\mu}_1^{pre}$, $\hat{\sigma}_1^{pre}$
Choice rule 2	α, β, φ	Fixed: v_1	β, φ	Fixed: $\hat{\lambda}$, $\hat{\vartheta}$, $\hat{\sigma}_o^2$, $\hat{\sigma}_d^2$, $\hat{\mu}_1^{pre}$, $\hat{\sigma}_1^{pre}$
Choice rule 3	α, β, φ	Fixed: v_1	β, φ	Fixed: $\hat{\lambda}$, $\hat{\vartheta}$, $\hat{\sigma}_o^2$, $\hat{\sigma}_d^2$, $\hat{\mu}_1^{pre}$, $\hat{\sigma}_1^{pre}$
Choice rule 4	α, β, ρ	Fixed: v_1	β, φ	Fixed: $\hat{\lambda}$, $\hat{\vartheta}$, $\hat{\sigma}_o^2$, $\hat{\sigma}_d^2$, $\hat{\mu}_1^{pre}$, $\hat{\sigma}_1^{pre}$
Choice rule 5	α, β, ρ, φ	Fixed: v_1	β, ρ	Fixed: $\hat{\lambda}$, $\hat{\vartheta}$, $\hat{\sigma}_o^2$, $\hat{\sigma}_d^2$, $\hat{\mu}_1^{pre}$, $\hat{\sigma}_1^{pre}$
Choice rule 6	α, β, ρ, φ	Fixed: v_1	β, φ, ρ	Fixed: $\hat{\lambda}$, $\hat{\vartheta}$, $\hat{\sigma}_o^2$, $\hat{\sigma}_d^2$, $\hat{\mu}_1^{pre}$, $\hat{\sigma}_1^{pre}$
Choice rule 7			β, φ, ρ	Fixed: $\hat{\lambda}$, $\hat{\vartheta}$, $\hat{\sigma}_o^2$, $\hat{\sigma}_d^2$, $\hat{\mu}_1^{pre}$, $\hat{\sigma}_1^{pre}$
Choice rule 8			β, φ, ρ	Fixed: $\hat{\lambda}$, $\hat{\vartheta}$, $\hat{\sigma}_o^2$, $\hat{\sigma}_d^2$, $\hat{\mu}_1^{pre}$, $\hat{\sigma}_1^{pre}$

Model estimation and comparison

Models were fit using Stan and the rSTAN package (Stan Development Team, 2022) in R (Version 4.1.1). To fit single subject models to human and RNN data, we ran 2 chains with 1000 warm-up samples. Chain convergence was assessed via the Gelman-Rubinstein convergence diagnostic $\hat{R}$ and sampling continued until 1 ≤ $\hat{R}$ ≤ 1.02 for all parameters. 1000 additional samples were then retained for further analysis.

Model comparison was performed using the loo-package in R (Vehtari et al., 2022) and the Widely-Applicable Information Criterion (WAIC), where lower values reflect a superior model fit (Vehtari et al., 2017). WAICs were computed for each model and human subject/ RNN instance. RNN model comparison focused on the model architecture with the lowest

cumulative regret (see Eq. 37). For visualization purposes, we calculated delta WAIC scores for each model by first summing WAIC values for each model over all participants/RNN instances and then subtracting the summed WAIC value of the winning model (Model with the lowest WAIC value if summed over all participants/RNN instances).

Cumulative regret

Task performance was quantified using *cumulative regret*, i.e. the cumulative loss due to the selection of suboptimal options, a canonical metric to compare RL algorithms in machine learning (Agrawal & Goyal, 2012; Auer et al., 2002; Wang et al., 2018). Formally, this corresponds to the difference between the reward of the optimal action ($\mathrm{R}_{\mathrm{a}^*,\mathrm{t}}$) and the obtained reward ($\mathrm{R}_{\mathrm{a}_\mathrm{t},\mathrm{t}}$), summed across trials:

$$Cumulative\ Regret = \sum_{t} \mathrm{R}_{\mathrm{a}^*,\mathrm{t}} - \mathrm{R}_{\mathrm{a}_\mathrm{t},\mathrm{t}} \tag{37}$$

Lower cumulative regret corresponds to better performance.

Hidden unit analysis

Deep learning algorithms like RNNs are often described as “black boxes” due to difficulties in understanding the mechanisms underlying their behavior (Sussillo & Barak, 2013). To address this issue, hidden unit activity was analyzed in relation to behavior via dimensionality reduction techniques, in particular principal component analysis (PCA) and targeted dimensionality reduction (TDR, Mante et al., 2013; Ebitz et al., 2018). PCA was used to obtain a first intuition about internal dynamics, and TDR was used to analyze interpretable dimensions of the hidden unit data.

For PCA, hidden unit values were first centered and standardized. Then, the time course of the first 3 principal components (PCs) was plotted for individual RNN instances, and color-coded according to chosen option, state-value estimate, and stay versus switch decisions. Across network instances, the first three PCs accounted for on average 73% of variance (see Supplemental Figure 1).

In contrast to PCA, TDR is a dimensionality reduction technique where the resulting high-dimensional neural activation data is projected onto axes with a specific interpretation. This is achieved by first using PCA to obtain an unbiased estimate of the most salient patterns of activations in the neural data and then regressing the resulting principle components against variables of interest. The resulting predicted values form the interpretable axes (Ebitz et al., 2018; Mante et al., 2013). Following previous work in primate neurophysiology (Ebitz et al.,

2018; Mante et al., 2013), for discrete variables (e.g. choice, stay/switch behavior) we used logistic regression:

$$p(choice = i|X) = \left(\frac{1}{1 + e^{-(X\beta_i)}}\right) \tag{38}$$

For continuous state-value estimates, we used linear regression:

$$\hat{Y} = \mathrm{B}_0 + X\mathrm{B}_1 \tag{39}$$

Here, X is are the principle components based on the standardized hidden unit predictor matrix of size N (no. of trials) x M (no. of hidden units) and $\mathrm{B}_0\ and\ \mathrm{B}_1$ are vectors of size M (no. of hidden units). The resulting axis ($\hat{Y}$), a vector of size no. of trials, now has a specific meaning - "Given the principle components on a given trial, what is the predicted value of the state-value-estimate?". For discrete outcomes, the PCA-based de-noised hidden unit data were projected onto a choice predictive (or stay/switch-predictive) axis by inverting the logistic link function, i.e. for the case of the choice axis:

$$choice\ axis_i = log\left(\frac{p(choice = i|X)}{1 - p(choice = i|X)}\right) = X\beta_i \tag{40}$$

The $choice\ axis_i$, a vector of size no.of trials, again has a concrete interpretation: "Given the de-noised hidden units on a trial, what are the log-odds of observing $choice_i$"? If the log odds are positive, it is more likely, if it's negative it is less likely to observe $choice_i$. If predicted occurrence and non-occurrence of $choice_i$ is equiprobable the log odds are 0.

To decode decisions from de-noised hidden unit activity, we used the results of the logistic regression (Equation 40) to calculate the probability of each action. The action with the maximum probability in a given trial was taken as the predicted action, and the proportion of correctly predicted choices was taken as the decoding accuracy.

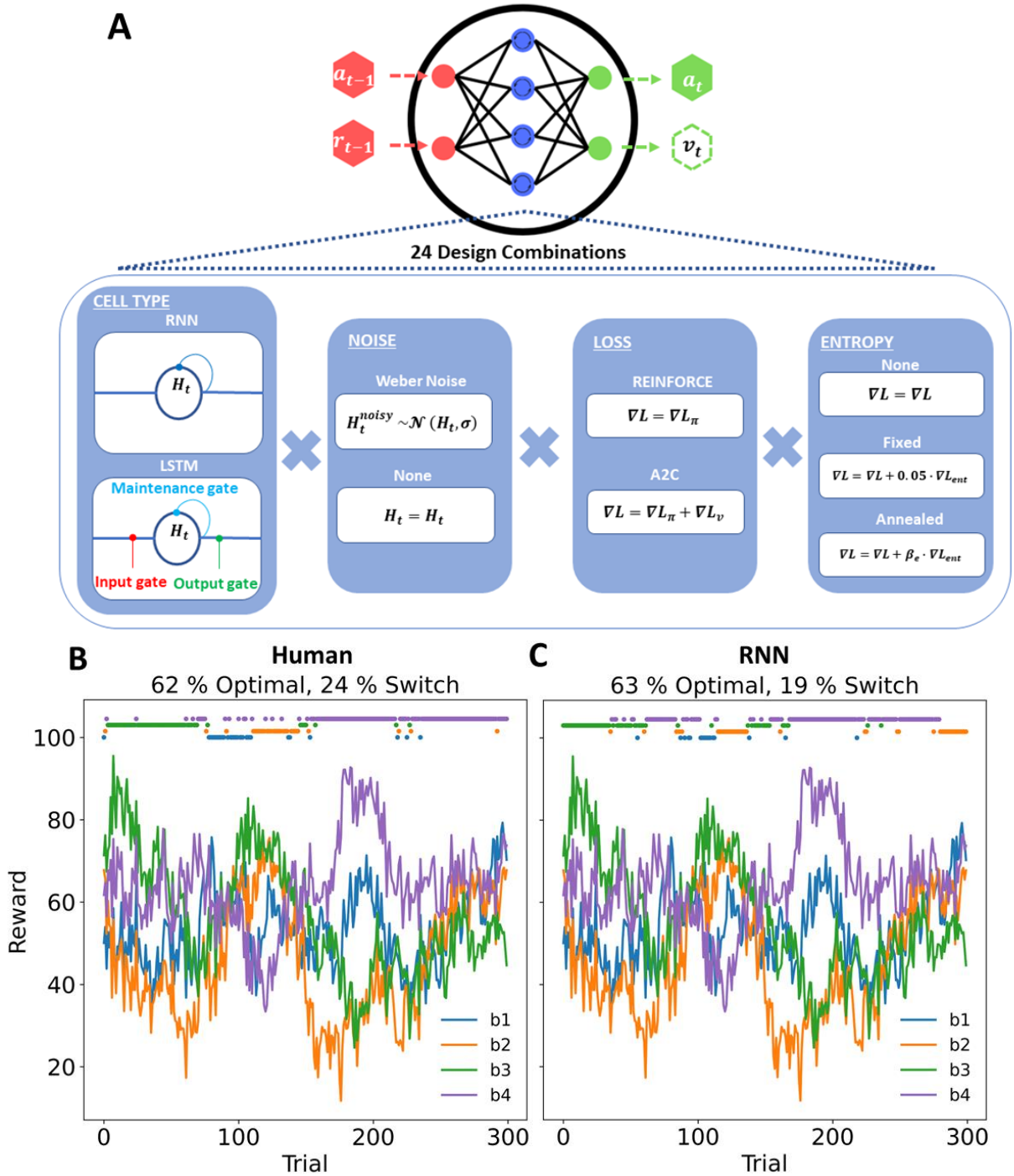

Figure 1. Artificial agent architectures and comparison of task performance to human agent. *(A) The input to the artificial agent is the previous reward (r_{t-1}) and the previous action (a_{t-1}) which is transformed within the hidden layer to output an action in the current trial (a_t) and an optional state-value estimate (v_t) (if the loss function is A2C). We systematically trained different network architectures varying in the factors Cell type (RNN or LSTM), Noise (Weber noise or none), Loss (REINFORCE or A2C) and Entropy (none, fixed or annealed) resulting in 24 design combinations (see methods section for details). (B) Example data from a human learner. (C) Example data from an LSTM network with computation noise solving the same task. In B and C, individual choices (colored dots on top) show selected action, and lines denote drifting rewards for each action. % Optimal: Proportion of choices of the most rewarding action. % Switches: Proportion of switches, i.e $choice_t$ not equal to $choice_{t-1}$.*

Results

Model-agnostic behavioral results

Our first aim was to identify the best-performing RNN architecture, as deep learning algorithms can be sensitive to hyperparameter settings (Haarnoja et al., 2019; Henderson et al., 2019). The factors considered in the RNN model space are summarized in Table 1. According to cumulative regret (Supplemental Figure 2), the best-performing architecture used LSTM units in combination with computation noise (Findling & Wyart, 2020). All subsequent analyses therefore focused on this architecture.

We next calculated cumulative regret for each agent (30 RNNs, 31 human subjects from the placebo condition of Chakroun et al., 2020) solving the identical bandit problem (see methods). A Bayesian t-test on the mean cumulative regret on the final trial showed moderate evidence for comparable performance of RNNs and human subjects ($BF_{01} = 4.274$). This was confirmed when examining the posterior distribution of the standardized effect size, which was centered at zero (*Mdn* = -0.008, Figure 2, B).

Analysis of switching behavior revealed that RNNs switched substantially less than human subjects (Bayesian Mann-Whitney U-Test $BF_{10} > 100$, Median switch probability: 31.5% (human), 14.5% (RNN)). To further compare switching behavior between RNNs and human subjects, all switch trials were classified according to number of unique bandits sampled since a particular switch target was last sampled. For example, in a bandit choice sequence of [1, 2, 2, 3, 1], two unique bandits have been sampled since bandit 1 was last sampled, which can be taken as a measure of the uncertainty associated with this bandit. Therefore, if an agent exhibits strategic (directed) exploration, this measure should overall be higher. Figure 2D shows that, in RNNs, switch proportions tend to decrease with uncertainty, as defined this way. In contrast, human switch proportions appeared more balanced (Figure 2D).

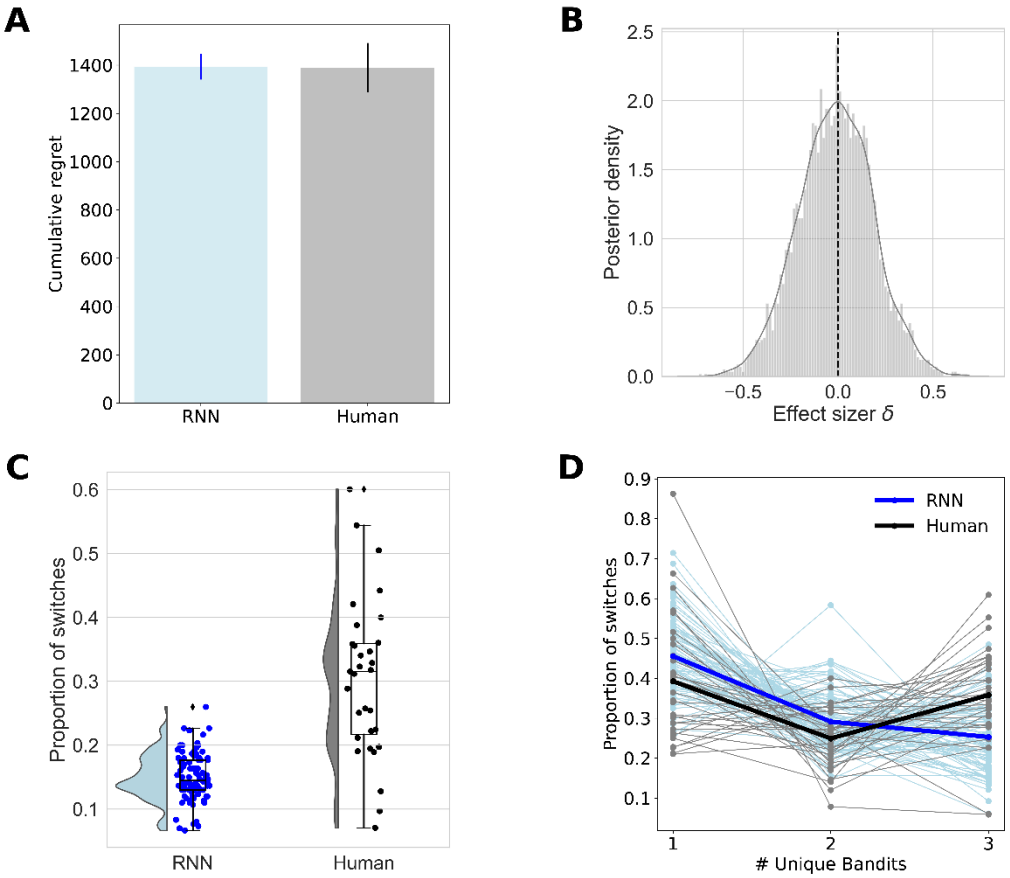

Figure 2. Behavioural data for LSTM networks with computation noise ("RNN", blue) and human learners (Chakroun et al., 2020, Placebo condition, black). *(A) Mean (+/- SEM) cumulative regret over trials for RNNs (blue) and human learners (black) (B) Posterior distribution of the standardized effect size (δ, Bayesian T-Test) showing moderate evidence against a difference in cumulative regret between RNNs and human learners ($BF_{01} = 4.274$).(C) Proportion of switches for RNNs (blue) and human learners (black). (D) Switch proportions sorted by number of unique bandits sampled between consecutive switch trials (x-axis), where higher numbers reflect higher uncertainty. Solid lines indicate means and thin lines indicate individual subject/instance data.*

Model comparison

To better understand human and RNN performance on those tasks, a total of 14 computational RL models (see methods section) were fitted to the behavioral data. All models were fitted to individual agent data (both RNN instances from the best-fitting architecture and human data from the placebo condition of Chakroun et al., 2020) via Hamiltonian monte Carlo as implemented in STAN. Model comparison was carried out using the Widely Applicable Information Criterion WAIC (Vehtari et al., 2017) by computing ΔWAIC scores for each model and agent (see methods section), yielding values of 0 for the best-fitting model. For both RNNs (Figure 3A) and human subject data (Figure 3B) the best-fitting model was a Bayesian-Learner

with perseveration and directed exploration terms (Eq. 8, SM+EP). For exact numerical values of ΔWAIC scores for each model and agent see Supplemental Table 1 and Supplemental Table 2. To quantify absolute model fit, the posterior predictive accuracy of this model was examined for each agent. To this end, 500 data sets were simulated from the model's posterior distribution, and the proportion of trials in which simulated and observed choices were consistent were computed and averaged across simulations. Predictive accuracy (Figure 4A) was higher for RNNs than for human agents (Human: $M = 0.673, SD = 0.119$; RNN: $M = 0.792$, $SD = 0.045$; $BF_{10} > 100$)

Analysis of model parameters

Next, we examined the model parameters (medians of individual subject posterior distributions) of the best fitting model and compared them between humans and artificial agents. Although the same model accounted for the data best, the resulting parameters differed considerably. Choice consistency (beta) was lower for RNNs than human data (Figure 4B, RNN: *Mdn* = 0.115, range: [0.001, 0.197], Human: *Mdn* = 0.185, range: [0.0434, 0.316]). Artificial agents showed substantially greater perseveration (Figure 4C, RNN: *Mdn* = 12.4, range: [3.88, 24.5], Human: *Mdn* = 5.59, range: [-1.60, 24.8]), and lower directed exploration (Figure 4D). While human subjects exhibited an exploration bonus parameter that was significantly positive, RNNs showed a negative exploration bonus (RNN: *Mdn* = -0.608, range: [-5.20, 0.718], Human: *Mdn* = 0.901, range: [-3.70, 5.93]).

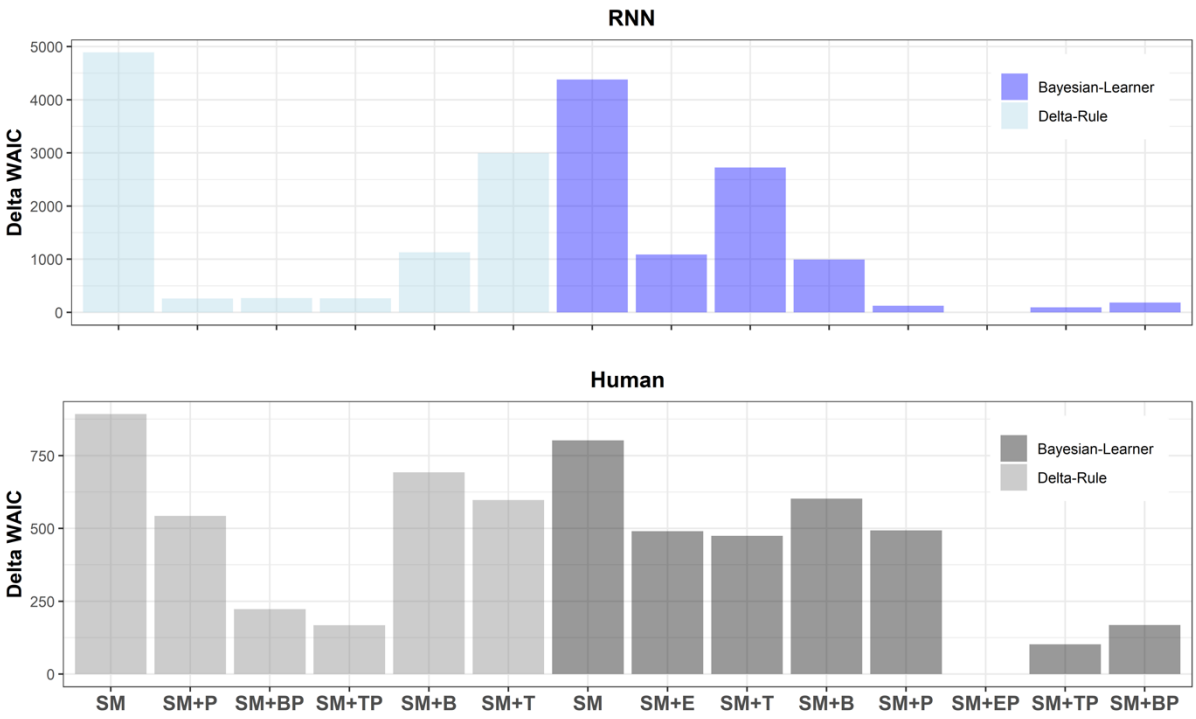

Figure 3. Model comparison via ΔWAIC (see methods section) where smaller values indicate a superior fit. *For both LSTM networks with computation noise (top panel) and human learners (bottom panel), the Bayesian learner with uncertainty and perseveration terms (SM+EP) accounted for the data best.*

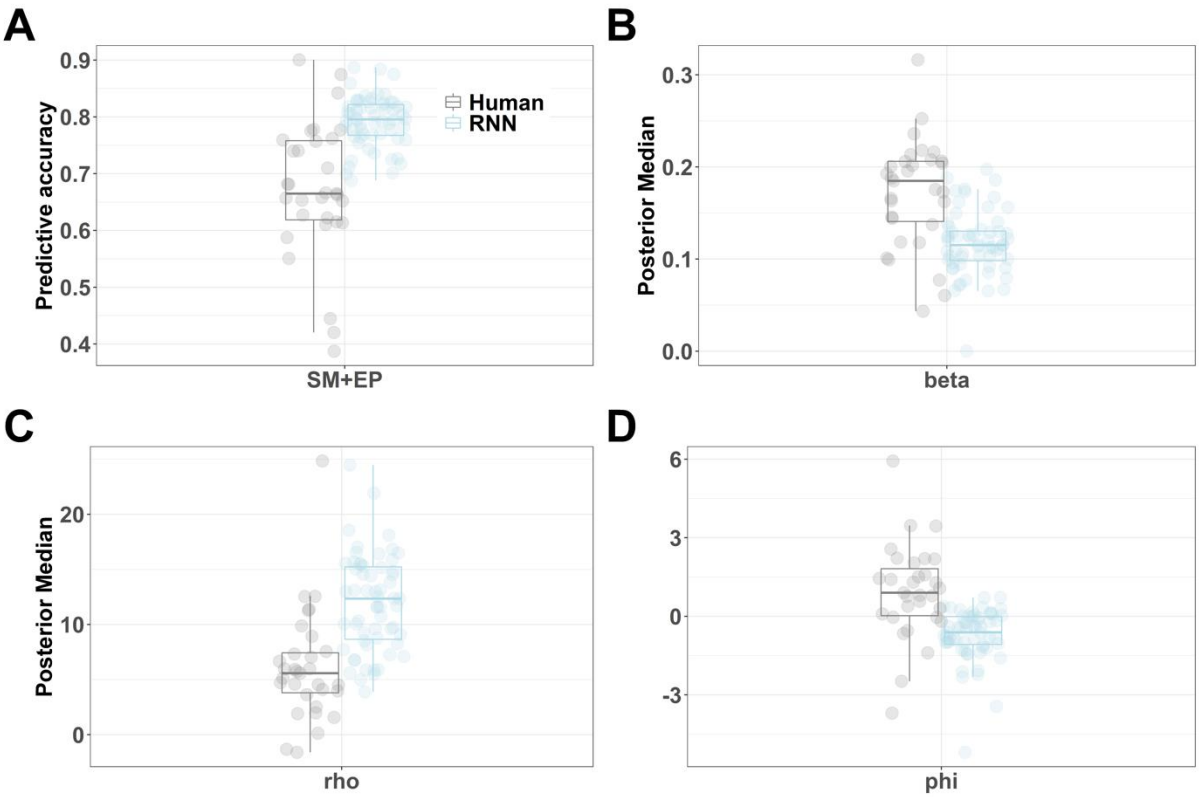

Figure 4. Median posterior values of model parameters for the best-fitting model (Bayesian learner with exploration and perseveration terms, SM+EP). *A: Predictive accuracy, B: choice stochasticity parameter beta , C: perseveration parameter rho, D: exploration parameter phi for human learners (black) and RNNs (blue).*

Hidden unit analysis

Finally, we investigated RNN hidden unit activity. This analysis is similar to the analysis of high dimensional neural data (Cunningham & Yu, 2014) and we first used PCA to visualize network dynamics. The first three principal components accounted for on average 73% of variance (see Supplemental Figure 1). The resulting network activation trajectories through principal component space were then examined with respect to behavioral variables. Coding network state by behavioral *choice* revealed separated choice-specific clusters in principal component space (see Figure 5A for hidden unit data from one instance, and see Supplement for the corresponding visualizations for all instances). The degree of spatial overlap of the choice-specific clusters directly related to the state-value estimate of the RNN (Figure 5B). Coding network state by stay vs. switch behavior (repeat previous choice vs. switch to another bandit, as a raw metric for exploration behavior, Figure 5C) revealed that switches predominantly occured in the region of activation space with maximum overlap in choice predictive clusters, corresponding to low state-value estimates. Highly similar effects were seen for all RNN instances investigated (see Supplement).

One downside of the PCA-analysis is that components are not readily interpretable. Therefore, targeted dimensionality reduction (TDR) (Mante et al., 2013) was applied, which projects the PCA-based de-noised hidden unit data onto novel axes with clear interpretations (see methods section).

To understand what the state-value estimate corresponds to in terms of observable choices and reward history, we used TDR to project the PCA-based de-noised hidden unit data onto a *value axis*, i.e. the predicted state-value estimate given the de-noised hidden unit activity on a given trial. This predicted state value (pooled across all trials from all network instances) was highly correlated with the reward obtained by the network on the previous trial ($r(17998) = .97$), Figure 5 D).

To examine the relationship between state-value estimates and stay-switch behaviour across all network instances examined, we projected the hidden unit data onto a *switch axis*, via logistic regression (see methods section), corresponding to the log-odds of observing a switch. Positive log-odds indicated that a switch decision is more likely than a stay decision, and vice versa for negative log-odds. Results confirmed the results from the analysis of single network instances (e.g. Figure 5B, C): switches predominantly occurred when estimated state value was low, as reflected in a negative correlation of the *value axis* and the *switch axis* scores ($r(17998) = -.80$).

Further we asked whether switching occurs randomly, or follows a predictable pattern. To this end, a multinomial model was fitted to predict RNN choices given the current PCA-based de-noised hidden unit activity. We then compared the accuracy of choice prediction between stay and switch trials. If RNNs follow a switching strategy, the accuracy of predicting switching decisions from de-noised hidden unit activity should be above chance level (0.25). The prediction accuracy was near perfect for stay decisions (*M*=0.996, see Figure 5F) and markedly disrupted but still substantially above chance level for switch decisions (*M*=0.702, see Figure 5F). This is consistent with the idea that RNNs rely on more than choice randomization to solve the exploration-exploitation dilemma.

We next explored how RNNs select which option to explore during switch trials. To this end, we compared switch targets (the option selected on a switch trial) to switch non-targets (the other bandits not selected on a switch-trial). A first comparison focused on the last observed reward, and as second analysis focused on uncertainty (based on the trialwise-heuristic, Eq. 30). Across RNN instances, we computed the mean rank of switch-targets and mean ranks of switch non-targets with respect to these two variables. A rank of 2 corresponds to selecting the highest valued bandit, and a rank of 0 corresponds to selecting the lowest valued badit. Therefore, the expected value of a random choice from the ranks ([0,1,2]) would be 1. Mean ranks higher or lower than 1 can thus be interpreted as switch-targets being biased towards higher or lower ranked bandits, respectively. Indeed, RNNs show a tendency to switch

to bandits with higher previous rewards (Figure 6, A) and lower uncertainty (Figure 6, B). Furthermore, in analogy to the analysis of behavioural data (Figure 2, D), the prediction accuracy of switch choices given the de-noised hidden units was better for less uncertain bandits (Supplemental Figure 4).

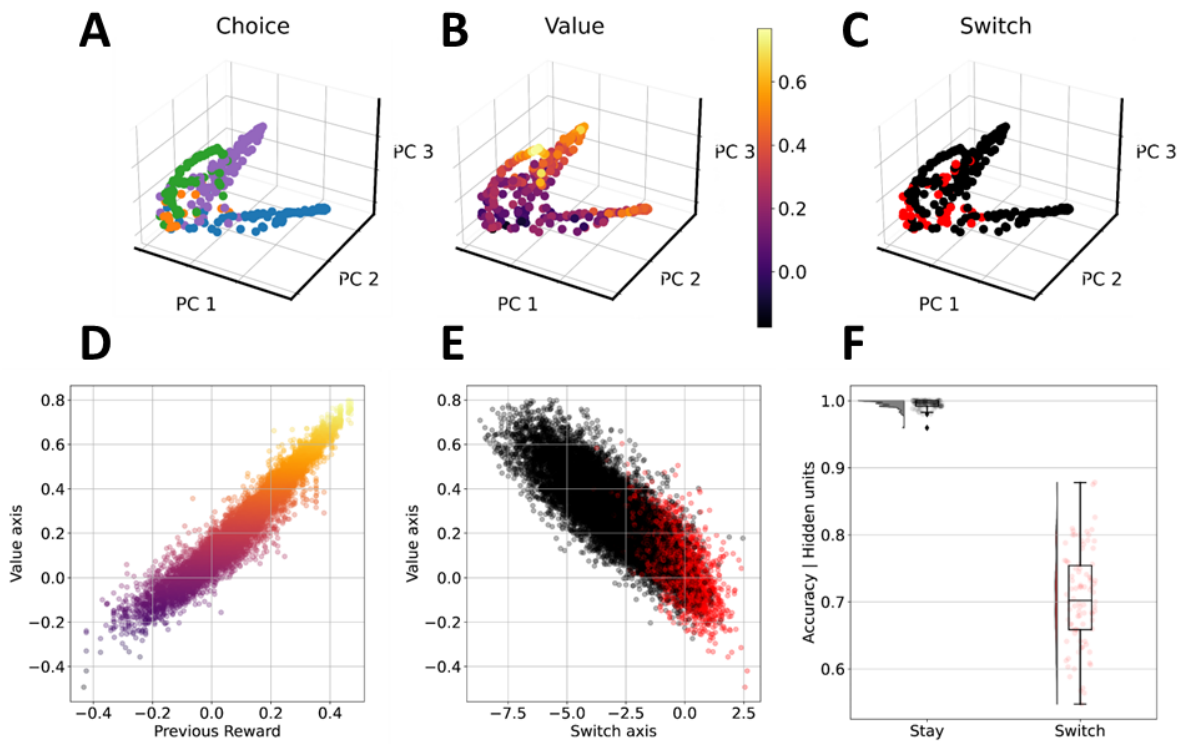

Figure 5. Hidden unit activation dynamics for a single network instance (A-C) and across all instances (D, E). A-C: *Hidden unit dynamics (first three principal components) of an example RNN agent color coded by choice (A), state-value estimate (B) and switching behavior (C, switch – red, stay - black). D, E: Targeted dimensionaility reduction. D: The state-value axis (y-axis) was highly correlated with previous reward (x-axis). D: Lower state-value (y-axis) was linked to greater log-odds of switching (x-axis). F: Accuracy of choice prediction given the PCA-based de-noised hidden unit activation state using a multinomial model revealed almost perfect accuracy for stay decisions (99%) and reduced, but above chance-level accuracy for switch decisions (70%).*

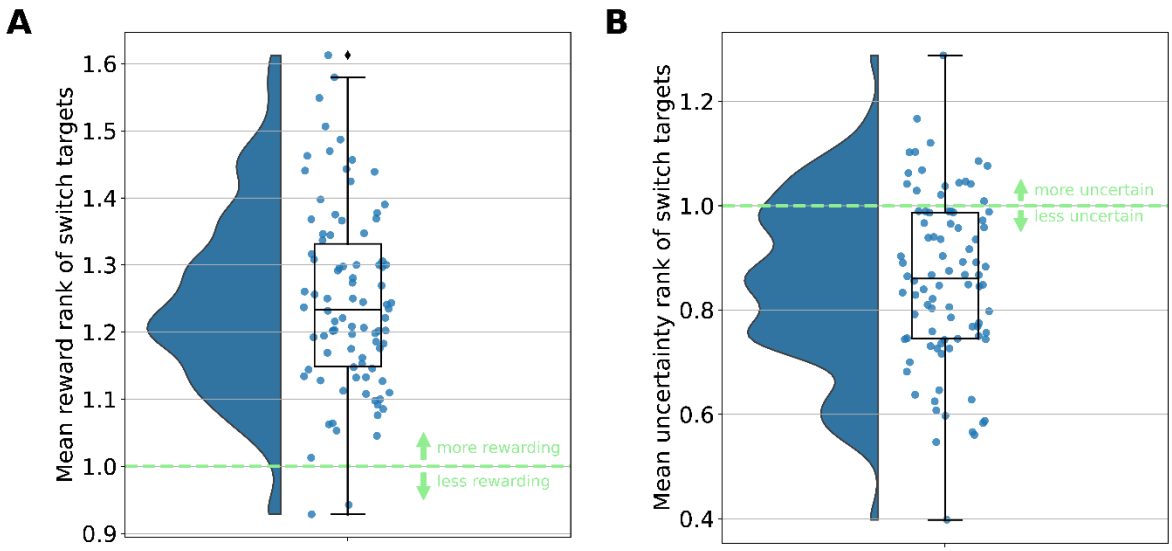

Figure 6. Switch-target analysis regarding previous reward (A) and uncertainty (B). *On a given switch trial the last observed reward and uncertainty of all 3 switch options were ranked (0=lowest, 2 = highest). Points denote the mean rank of the switch-target across all switch trials per RNN instance. Values below or above 1 denote a switch bias towards lower or higher ranked bandits, respectively. RNNs show substantial evidence to switch to higher valued (A) and less uncertain bandits (B).*

Discussion

Here we comprehensively investigated exploration mechanisms in recurrent neural network models during reinforcement learning in volatile environments. We expanded upon previous work in four ways. First, in contrast to earlier work (Findling & Wyart, 2020; Wang et al., 2018) we focused on four-armed restless bandit problems, allowing for a more comprehensive analysis of exploration behavior. Second, we systematically investigated a range of neural network design choices and resulting impacts on performance. Third, we directly compared human and RNN behavior, both in terms of performance (cumulative regret) and using computational modeling, when solving the exact same task problem. Finally, we investigated exploration mechanisms in the best-performing network architecture via a comprehensive analysis of hidden unit activation dynamics.

We extensively tested and transparently report upon a total of 24 RNN design factor combinations. The architecture exhibiting best performance was an LSTM network, combined with computation noise as previously suggested (Findling & Wyart, 2020), no Entropy regularization and trained with the advantage-actor-critic (A2C) algorithm (Mnih et al., 2016). The superior performance of the LSTM verus the vanilla RNN is not suprising. LSTMs are endowed with a more sophisticated memory process (Equations 5 - 9) where different gating mechanisms regulate the impact of past experiences (previous actions and rewards) on current decisions. These mechanisms allow LSTM networks to learn dependencies over

longer time scales than vanilla RNNs (Hochreiter & Schmidhuber, 1997). The performance benefit of LSTMs also resonates with a well-known computational model of learning and action selection mechanisms in prefrontal cortex (PFC) and basal ganglia (O'Reilly & Frank, 2006). This model is characterized by a combination of LSTM-like gating mechanisms that are combined with an Actor-Critic architecture. Here, the *Actor* (i.e., the basal ganglia) updates actions by gating working memory updating processes in the PFC. The *Critic* (i.e., midbrain DA neurons) estimates reward values of possible actions, thereby adjusting future actions to maximize reward. Similar to Findling & Wyart (2020) our results show that biologically-inspired computation noise ("Weber Noise", Findling & Wyart, 2020) is a superior noise mechanism than entropy regularization, at least in the context of this task. The rationale behind entropy regularization is to add noise to the policy during training to discourage premature convergence to a suboptimal policy (Mnih et al., 2016). In contrast, Weber noise (Findling & Wyart, 2020) is noise added to hidden unit activity that scales with the degree of recurrent activity reconfiguration between subsequent trials. This "update-dependent" mechanism might thus entail exploration-specific noise that contrasts with the introduction of general stochasticity as implemented in entropy regularization schemes. This result further reinforces the perfomance-enhancing effect of computation noise observed in human reward-guided decision making (Findling et al., 2019) which is thought to be modulated by reciprocal connections of the locus coeruleus-norepinephrine system and the anterior cingulate cortex (Findling & Wyart, 2021; McClure et al., 2005). This also resonates with results from deep neural networks, were various noise-based schemes have been implemented to improve network performance and/or to increase the resilience of the networks under sparse information, e.g. noise at the input level, similar to dataset augmentation methods (Goodfellow et al., 2016), at the level of the weight update (An, 1996) or during computation (Dong et al., 2020; Fortunato et al., 2019; Qin & Vucinic, 2018).

To better understand differences between human and neural network behavior, we applied comprehensive cognitive modeling (Farrell & Lewandowsky, 2018). Model comparison according to WAIC revealed that RNN and human behaviour were best accounted for by the same model: a bayesian learning rule (Kalman Filter, Chakroun et al., 2020; Daw et al., 2006; Kalman, 1960; Wiehler et al., 2021) combined with a softmax choice rule (SM+EP) incorporating a perseveration bonus (ρ) and a directed exploration term (φ) modeling an "exploration bonus" for uncertain options. This model was previously found to account best for human data from the same restless bandit task (Chakroun et al., 2020; Wiehler et al., 2021), and exhibits good parameter and model recovery properties (Danwitz et al., 2022). Humans and artifical agents alike appear to estimate the underlying reward generating process from observed rewards of the bandits. In contrast to a constant learning rate in the delta rule models, in this model, the learning rate (kalman gain) varies from trial to trial, such that the

degree of updating scales with a bandit's uncertainty. This suggests that RNNs and human subjects dynamically modulate the influence of past actions and rewards to current decisions according to an estimate of the uncertainty of a bandit. However, additional modeling revealed that the exact formalism used to model directed exploration may be negligible, since models with a trial-based exploration term (SM+TP) and a bandit-identiy-based exploration term (SM+BP) show similar patterns of directed exploration difference between humans vs. RNNs (See Supplemental Figure 3).

Analysis of model parameters then revealed a tendency for uncertainty aversion in RNNs, reflected in an overall *negative* exploration bonus parameter φ (i.e., an "exploration malus"). In contrast, human learners typically show a positive effect of uncertainty on choice probabilities (directed exploration) (Chakroun et al., 2020; Schulz et al., 2019; Schulz & Gershman, 2019; Wiehler et al., 2021; Wilson et al., 2014, 2021). This divergence between human and artificial agent behavior suggests that directed exploration is not required for human-level task performance. Recent simulation work showed an inverted u-shaped influence of φ on reward accumulation (Danwitz et al., 2022) such that insufficient or excessive directed exploration are detrimental for performance. Directed exploration parameters of human subjects in this study (see Figure 4D) appear to scatter around the optimal point of the inverted u-shaped function of the simulation study (Figure 3C from Danwitz et al., 2022). One possibility is that RNNs compensate for a lack of directed exploration via excessive perseveration behavior, that is, the negative φ estimates in RNNs (reflecting uncertainty aversion) might reflect higher-order perseveration. The SM+EP model accounts for first-order perseveration, but RNNs might perseverate not only on the basis of the previous choice ($choice_{t-1}$) but also with respect to a longer choice history. Variance attributable to n-trial back perseveration could drive a negative φ parameter. Several models account for higher-order perseveration (Kovach et al., 2012; Lau & Glimcher, 2005; Miller et al., 2019) and future work could expand the model space further to examine these effects in RNN and human agents during restless multi-armed bandit tasks.

However, even for first-order perseveration, RNNs showed substantially higher levels of perseveration than human subjects. According to the median parameter estimates, repeating the previous choice increases the value of a bandit by 12.36 (range [3.88, 24.46]) reward points for RNN agents and by 5.59 (range [-1.6, 24.83]) reward points for human agents. Perseveration is often thought to be maladaptive, as learners "stick" to choices regardless of reward or task demands (Dehais et al., 2019; Hauser, 1999; Hotz & Helm-Estabrooks, 1995). For example, increased levels of perseveration are a hallmark of depression and substance use disorders (Zuhlsdorff, 2022), behavioral addictions (de Ruiter et al., 2009), obsessive compulsive disorder (Apergis-Schoute & Ip, 2020) and are tightly linked to intact PFC functioning (Goldberg & Bilder, 1987; Munakata et al., 2003). In the light

of these findings, it might appear suprising that RNN agents show such a pronounced tedency to perseverate. But perseveration might support reward accumulation by enabling the network to minimize losses due to excessive exploration. In contrast, human agents perseverate less and explore more (Figure 2C), thereby avoiding the costs of prolonged perseveration and finding the optimal bandit faster by continuously exploring the environment. Both strategies converge on comparable performance. Lastly, RNNs showed a lower inverse temperature parameter (β) than human learners. All things being equal, lower values of β values reflect more random action selection, such that choices depent less on the terms included in the model. A β-value of zero would indicate completely random choices, and as β-values increase, the policy would approach a deterministic policy in which choices depend completely upon the model terms. However, the absolute level of choice stochasticity reflected in a given value of β also depends on the other terms in the model. Whereas the absolute magnitude of value and exploration terms was comparable between human and RNNs, the perseveration term was about twice the magnitude in RNNs, which explains the lower β-values in RNNs. The results from the analysis of predictive accuracy also confirmed that a greater proportion of choices was accounted for by the best-fitting computational model in RNNs compared to humans, showing that these differences in β do not reflect a poorer model fit.

To investigate the computational dynamics underlying RNN behaviour, we initially applied dimensionality reduction of hidden unit activations patterns via Principal Component Analysis (PCA) (Findling & Wyart, 2020; Mante et al., 2013; Wang et al., 2018). The first three principal components accounted for on average 73% of variance in hidden unit activity (see Supplemental Figure 1). Visual inspection of activation patterns in principal component space then revealed three effects: First, coding network state by behavioral *choice* revealed clearly separated choice-specific clusters in principal component space, an effect that was observed across all RNN instances examined (see Supplement). Second, the degree of spatial overlap of the choice-specific clusters directly related to the state-value estimate of the network. Action representations on trials with higher state-value estimates were more seperated than during trials with lower state-value estimates. Again, this pattern was observed across all RNN instances examined (see Supplement) and resonates with systems neuroscience work showing neural populations are more predictive for high-value actions than for low-value actions (Ebitz et al., 2018). Oculomotor regions like the frontal eye field (FEF) (Ding & Hikosaka, 2006; Glaser et al., 2016; Roesch & Olson, 2003, 2007) and the lateral intraparietal area (LIP) (Platt & Glimcher, 1999; Sugrue et al., 2004) show more pronounced choice-predictive activation patterns during saccades to high vs. low value targets. Third, to investigate the link between RNN dynamics and exploration, we coded network state in PC-space by stay vs. switch behavior. This revealed that switches predominantly occured in the region of activation space with maximum overlap in choice predictive clusters, corresponding

to low state-value estimates. Again, this effect was observed across all network instances examined. Generally, these observations show that 1) switches occurred predominantly during trials with low state value, 2) low state value was associated with less pronounced choice-predictive activation patterns. Although these patterns were qualitatively highly similar across RNN instances (see Supplement), the geometrical embedding of these effects in principal component space differed. This illustrates one downside of PCA - the components as such are not directly interpretable, and the different rotations of patterns in principal component space complicate the aggregation of analyses across network instances.

To address this issue, and to obtain interpretable axes, we applied targeted dimensionality reduction (TDR) (Ebitz et al., 2018; Mante et al., 2013). TDR projects the PCA-based de-noised hidden unit activation patterns onto novel axes with clear interpretations (see methods section), allowing for a quantification of the intuitions gained from PCA. We projected the de-noised hidden unit data onto a *value axis*, i.e. the predicted state-value estimate given the de-noised hidden unit activity on a given trial. Across all network instances, this measure was highly correlated with the reward obtained on the previous trial (Figure 5D). Likewise, we projected the de-noised hidden unit data onto a *switch-axis*, i.e. the predicted log-odds of observing a switch, given the de-noised hidden unit activity on a given trial. Across all network instances, this axis showed a strong negative correlation with the value-axis, confirming that indeed the log-odds of switching increased with decreasing state value, and decreased with increasing state value, resembling a Win-Stay-Lose-Shift (WSLS) strategy (Herrnstein, 1997) that accounts for substantial choice proportions also in human work (Worthy et al., 2013). However, pure WSLS would predict much higher switch rates than observed in RNNs, suggesting that RNNs show a mixture of a WSLS-like strategy in conjunction with high perseveration.

Finally, we decoded choices from de-noised hidden unit activation dynamics, and compared prediction accuracy for stay vs. switch decisions. The decoder showed near perfect accuracy for stay decisions, which resonates with animal work showing that neural choice decoding is improved during perseveration (Coe et al., 2002; Ebitz et al., 2018). Importantly, performance of the decoder was lower, but still substantially above chance-level for switches. The de-noised hidden units therefore represent an activation pattern that can be utilized to correctly predict switch-targets, suggesting that switching behavior is not entirely based on choice randomization. Further analyses revealed that RNNs tended to switch to bandits with higher previous reward and lower uncertainty. Switching to bandits with higher observed rewards could be explained by value-based exploration ("Boltzman Exploration", Sutton & Barto, 2018) as implemented in standard RL-models with a softmax action selection function, where choice probabilities are proportional to trial-by-trial value estimates. As probabilities in the softmax function sum to 1, decreases in the value of one bandit increase the choice

probabilities of other bandits proportional to their value estimates. Switching to bandits with lower uncertainty resonates with our cognitive modeling results showing negative exploration bonus parameters in the networks. Generally, these findings confirm that RNNs explore in an uncertainty averse and value-based manner, in contrast to human agents, who show a postive exploration bonus.

One caveat of this work is that, although often applied in the context of RL in volatile environments (Domenech et al., 2020; Kovach et al., 2012; Swanson et al., 2020), the comparison between stay and switch trials does not unequivocally map onto the exploitation vs. exploration distinction. For example, stay decisions can be due to greedy choices (choosing the option with the highest expected reward) but also due to perseveration. In contrast, switch decisions can be due to random or strategic exploration (Wilson et al., 2021) and may involve more complex model-based strategies and/or simpler heuristics like following motor patterns such as exploring by choosing each available option once and then exploiting (Fintz et al., 2022). We nonetheless applied the stay vs. switch distinction, as it makes by far the least assumptions regarding what constitutes exploration vs. exploration.

Several limitations of this work need to be adressed. First, although our final network model space resulted in a total of 24 different RNN architectures, the impact of additional design choices such as network size, learning rate, discount factor, type of activation function or values for the Weber fraction (noise) were not systematically explored. Although the combination of LSTM with the A2C algorithm is robust to different hyperparameter settings (Mnih et al. 2016), a different RNN architecture or hyperparameter combination could have yielded even better performance or could have produced a form of directed exploration. Future research could benefit from the use of other architectures such as transformer models (Chen et al., 2021; Parisotto et al., 2020; Upadhyay et al., 2019) or explore the role of these additional factors. Second, a general limitation of this approach more generally is that neural network models, although roughly based on neuronal computations, suffer from a number of biological implausibilities (Pulvermüller et al., 2021). These include the backpropagation algorithm used to update the parameters of the network (Lillicrap et al., 2020), the lack of separate modules analogious to different brain regions, and lack of neuromodulation mechanisms (Pulvermüller et al., 2021). However, some recent work has begun to adress these shortcomings (Mei et al., 2022; Robertazzi et al., 2022). Third, as outlined above, the negative exploration bonus that we observed in RNNs could be due to higher-order perseveration, i.e. perseveration behavior beyond the last trial, which would then result in a negative φ (see also Chakroun et al., 2020). Such higher-order perseveration was discussed in theoretical work (Miller et al., 2019) and observed in rats (Miller et al., 2019) and monkeys (Lau & Glimcher, 2005). Future work might benefit from exploring mechanisms underlying different types of perseveration more extensively.

Taken together, we identified a novel RNN architecture (LSTM with computation noise) that solved restless four-armed bandit tasks with human-level accuracy. Computational modeling revealed that the same computational model (Bayesian Learner model with directed exploration and perseveration terms) accounted for human and RNN behavior best. However, in contrast to human learners, who exhibited a postive exploration bonus parameter φ, in RNNs, this parameter was instead negative, reflecting uncertainty avoidance and/or higher-order perseveration. First-order perseveration behavior was likewise substantially increased in artifical agents. Further analyses of the networks' exploration behavior confirmed that exploratory choices were primarily driven by rewards and choice history. Hidden-unit dynamics revealed that exploration behavior in RNNs was driven by a disruption of choice predictive signals during states of low estimated state value, reminiscent of computational mechanisms in monkey PFC. Overall, our results highlight how computational mechanisms in RNNs can at the same time converge with and diverge from findings in human neuroscience.

References

Agrawal, S., & Goyal, N. (2012). *Analysis of Thompson Sampling for the multi-armed bandit problem* (arXiv:1111.1797). arXiv. https://doi.org/10.48550/arXiv.1111.1797

An, G. (1996). The Effects of Adding Noise During Backpropagation Training on a Generalization Performance. *Neural Computation*, *8*(3), 643–674. https://doi.org/10.1162/neco.1996.8.3.643

Apergis-Schoute, A., & Ip, H. Y. S. (2020). Reversal Learning in Obsessive Compulsive Disorder: Uncertainty, Punishment, Serotonin and Perseveration. *Biological Psychiatry*, *87*(9), S125–S126. https://doi.org/10.1016/j.biopsych.2020.02.339

Auer, P., Cesa-Bianchi, N., & Fischer, P. (2002). Finite-time Analysis of the Multiarmed Bandit Problem. *Machine Learning*, *47*(2), 235–256. https://doi.org/10.1023/A:1013689704352

Beharelle, A. R., Polanía, R., Hare, T. A., & Ruff, C. C. (2015). Transcranial Stimulation over Frontopolar Cortex Elucidates the Choice Attributes and Neural Mechanisms Used to

Resolve Exploration–Exploitation Trade-Offs. *Journal of Neuroscience*, *35*(43), 14544–14556. https://doi.org/10.1523/JNEUROSCI.2322-15.2015

Behrens, T. E. J., Woolrich, M. W., Walton, M. E., & Rushworth, M. F. S. (2007). Learning the value of information in an uncertain world. *Nature Neuroscience*, *10*(9), Article 9. https://doi.org/10.1038/nn1954

Binz, M., & Schulz, E. (2022). *Using cognitive psychology to understand GPT-3* (arXiv:2206.14576). arXiv. https://doi.org/10.48550/arXiv.2206.14576

Botvinick, M., Ritter, S., Wang, J. X., Kurth-Nelson, Z., Blundell, C., & Hassabis, D. (2019). Reinforcement Learning, Fast and Slow. *Trends in Cognitive Sciences*, *23*(5), 408–422. https://doi.org/10.1016/j.tics.2019.02.006

Botvinick, M., Wang, J. X., Dabney, W., Miller, K. J., & Kurth-Nelson, Z. (2020). Deep Reinforcement Learning and Its Neuroscientific Implications. *Neuron*, *107*(4), 603–616. https://doi.org/10.1016/j.neuron.2020.06.014

Chakroun, K., Mathar, D., Wiehler, A., Ganzer, F., & Peters, J. (2020). Dopaminergic modulation of the exploration/exploitation trade-off in human decision-making. *ELife*, *9*, e51260. https://doi.org/10.7554/eLife.51260

Chen, L., Lu, K., Rajeswaran, A., Lee, K., Grover, A., Laskin, M., Abbeel, P., Srinivas, A., & Mordatch, I. (2021). Decision Transformer: Reinforcement Learning via Sequence Modeling. *Advances in Neural Information Processing Systems*, *34*, 15084–15097. https://proceedings.neurips.cc/paper/2021/hash/7f489f642a0ddb10272b5c31057f0663-Abstract.html

Coe, B., Tomihara, K., Matsuzawa, M., & Hikosaka, O. (2002). Visual and Anticipatory Bias in Three Cortical Eye Fields of the Monkey during an Adaptive Decision-Making Task. *Journal of Neuroscience*, *22*(12), 5081–5090. https://doi.org/10.1523/JNEUROSCI.22-12-05081.2002

Cunningham, J. P., & Yu, B. M. (2014). Dimensionality reduction for large-scale neural recordings. *Nature Neuroscience*, *17*(11), 1500–1509. https://doi.org/10.1038/nn.3776

Danwitz, L., Mathar, D., Smith, E., Tuzsus, D., & Peters, J. (2022). Parameter and Model Recovery of Reinforcement Learning Models for Restless Bandit Problems. *Computational Brain & Behavior*, *5*(4), 547–563. https://doi.org/10.1007/s42113-022-00139-0

Dasgupta, I., Wang, J., Chiappa, S., Mitrovic, J., Ortega, P., Raposo, D., Hughes, E., Battaglia, P., Botvinick, M., & Kurth-Nelson, Z. (2019). *Causal Reasoning from Meta-reinforcement Learning* (arXiv:1901.08162). arXiv. https://doi.org/10.48550/arXiv.1901.08162

Daw, N. D., O'Doherty, J. P., Dayan, P., Seymour, B., & Dolan, R. J. (2006). Cortical substrates for exploratory decisions in humans. *Nature*, *441*(7095), Article 7095. https://doi.org/10.1038/nature04766

de Ruiter, M. B., Veltman, D. J., Goudriaan, A. E., Oosterlaan, J., Sjoerds, Z., & van den Brink, W. (2009). Response Perseveration and Ventral Prefrontal Sensitivity to Reward and Punishment in Male Problem Gamblers and Smokers. *Neuropsychopharmacology*, *34*(4), Article 4. https://doi.org/10.1038/npp.2008.175

Dehais, F., Hodgetts, H. M., Causse, M., Behrend, J., Durantin, G., & Tremblay, S. (2019). Momentary lapse of control: A cognitive continuum approach to understanding and mitigating perseveration in human error. *Neuroscience & Biobehavioral Reviews*, *100*, 252–262. https://doi.org/10.1016/j.neubiorev.2019.03.006

Ding, L., & Hikosaka, O. (2006). Comparison of Reward Modulation in the Frontal Eye Field and Caudate of the Macaque. *Journal of Neuroscience*, *26*(25), 6695–6703. https://doi.org/10.1523/JNEUROSCI.0836-06.2006

Domenech, P., Rheims, S., & Koechlin, E. (2020). Neural mechanisms resolving exploitation-exploration dilemmas in the medial prefrontal cortex. *Science*, *369*(6507), eabb0184. https://doi.org/10.1126/science.abb0184

Dong, Z., Oktay, D., Poole, B., & Alemi, A. A. (2020). *On Predictive Information in RNNs* (arXiv:1910.09578). arXiv. https://doi.org/10.48550/arXiv.1910.09578

Drugowitsch, J., Wyart, V., Devauchelle, A.-D., & Koechlin, E. (2016). Computational Precision of Mental Inference as Critical Source of Human Choice Suboptimality. *Neuron*, *92*(6), 1398–1411. https://doi.org/10.1016/j.neuron.2016.11.005

Ebitz, R. B., Albarran, E., & Moore, T. (2018). Exploration Disrupts Choice-Predictive Signals and Alters Dynamics in Prefrontal Cortex. *Neuron*, *97*(2), 450-461.e9. https://doi.org/10.1016/j.neuron.2017.12.007

Elman, J. L. (1990). Finding structure in time. *Cognitive Science*, *14*(2), 179–211. https://doi.org/10.1016/0364-0213(90)90002-E

Farrell, S., & Lewandowsky, S. (2018). *Computational Modeling of Cognition and Behavior*. Cambridge University Press. https://doi.org/10.1017/CBO9781316272503

Findling, C., Skvortsova, V., Dromnelle, R., Palminteri, S., & Wyart, V. (2019). Computational noise in reward-guided learning drives behavioral variability in volatile environments. *Nature Neuroscience*, *22*(12), 2066–2077. https://doi.org/10.1038/s41593-019-0518-9

Findling, C., & Wyart, V. (2020). *Computation noise promotes cognitive resilience to adverse conditions during decision-making* (p. 2020.06.10.145300). bioRxiv. https://doi.org/10.1101/2020.06.10.145300

Findling, C., & Wyart, V. (2021). Computation noise in human learning and decision-making: Origin, impact, function. *Current Opinion in Behavioral Sciences*, *38*, 124–132. https://doi.org/10.1016/j.cobeha.2021.02.018

Fintz, M., Osadchy, M., & Hertz, U. (2022). Using deep learning to predict human decisions and using cognitive models to explain deep learning models. *Scientific Reports*, *12*(1), Article 1. https://doi.org/10.1038/s41598-022-08863-0

Fortunato, M., Azar, M. G., Piot, B., Menick, J., Osband, I., Graves, A., Mnih, V., Munos, R., Hassabis, D., Pietquin, O., Blundell, C., & Legg, S. (2019). *Noisy Networks for Exploration* (arXiv:1706.10295). arXiv. https://doi.org/10.48550/arXiv.1706.10295

Glaser, J. I., Wood, D. K., Lawlor, P. N., Ramkumar, P., Kording, K. P., & Segraves, M. A. (2016). Role of expected reward in frontal eye field during natural scene search. *Journal of Neurophysiology*, *116*(2), 645–657. https://doi.org/10.1152/jn.00119.2016

Goldberg, E., & Bilder, R. M. (1987). The Frontal Lobes and Hierarchical Organization of Cognitive Control. In *The Frontal Lobes Revisited*. Psychology Press.

Goodfellow, I., Bengio, Y., & Courville, A. (2016). *Deep learning*. MIT Press.

Haarnoja, T., Ha, S., Zhou, A., Tan, J., Tucker, G., & Levine, S. (2019). *Learning to Walk via Deep Reinforcement Learning* (arXiv:1812.11103). arXiv. https://doi.org/10.48550/arXiv.1812.11103

Hamid, A. A., Pettibone, J. R., Mabrouk, O. S., Hetrick, V. L., Schmidt, R., Vander Weele, C. M., Kennedy, R. T., Aragona, B. J., & Berke, J. D. (2016). Mesolimbic dopamine signals the value of work. *Nature Neuroscience*, *19*(1), Article 1. https://doi.org/10.1038/nn.4173

Hao, J., Yang, T., Tang, H., Bai, C., Liu, J., Meng, Z., Liu, P., & Wang, Z. (2023). *Exploration in Deep Reinforcement Learning: A Comprehensive Survey* (arXiv:2109.06668). arXiv. http://arxiv.org/abs/2109.06668

Hauser, M. D. (1999). Perseveration, inhibition and the prefrontal cortex: A new look. *Current Opinion in Neurobiology*, *9*(2), 214–222. https://doi.org/10.1016/S0959-4388(99)80030-0

Henderson, P., Islam, R., Bachman, P., Pineau, J., Precup, D., & Meger, D. (2019). *Deep Reinforcement Learning that Matters* (arXiv:1709.06560). arXiv. https://doi.org/10.48550/arXiv.1709.06560

Herrnstein, R. J. (1997). *The matching law: Papers in psychology and economics* (pp. vi, 334). Harvard University Press.

Hochreiter, S., & Schmidhuber, J. (1997). Long Short-Term Memory. *Neural Computation*, *9*(8), 1735–1780. https://doi.org/10.1162/neco.1997.9.8.1735

Hotz, G., & Helm-Estabrooks, N. (1995). Perseveration. Part I: A review. *Brain Injury*, *9*(2), 151–159. https://doi.org/10.3109/02699059509008188

Huys, Q. J. M., Maia, T. V., & Frank, M. J. (2016). Computational psychiatry as a bridge from neuroscience to clinical applications. *Nature Neuroscience*, *19*(3), 404–413. https://doi.org/10.1038/nn.4238

Kalman, R. E. (1960). A New Approach to Linear Filtering and Prediction Problems. *Journal of Basic Engineering*, *82*(1), 35–45. https://doi.org/10.1115/1.3662552

Kovach, C. K., Daw, N. D., Rudrauf, D., Tranel, D., O'Doherty, J. P., & Adolphs, R. (2012). Anterior Prefrontal Cortex Contributes to Action Selection through Tracking of Recent Reward Trends. *The Journal of Neuroscience*, *32*(25), 8434–8442. https://doi.org/10.1523/JNEUROSCI.5468-11.2012

Kumar, S., Dasgupta, I., Marjieh, R., Daw, N. D., Cohen, J. D., & Griffiths, T. L. (2022). *Disentangling Abstraction from Statistical Pattern Matching in Human and Machine Learning* (arXiv:2204.01437). arXiv. https://doi.org/10.48550/arXiv.2204.01437

Ladosz, P., Weng, L., Kim, M., & Oh, H. (2022). Exploration in deep reinforcement learning: A survey. *Information Fusion*, *85*, 1–22. https://doi.org/10.1016/j.inffus.2022.03.003

Lake, B. M., Salakhutdinov, R., & Tenenbaum, J. B. (2015). Human-level concept learning through probabilistic program induction. *Science*, *350*(6266), 1332–1338. https://doi.org/10.1126/science.aab3050

Lau, B., & Glimcher, P. W. (2005). Dynamic Response-by-Response Models of Matching Behavior in Rhesus Monkeys. *Journal of the Experimental Analysis of Behavior*, *84*(3), 555–579. https://doi.org/10.1901/jeab.2005.110-04

LeCun, Y., Bengio, Y., & Hinton, G. (2015). Deep learning. *Nature*, *521*(7553), Article 7553. https://doi.org/10.1038/nature14539

Lillicrap, T. P., Santoro, A., Marris, L., Akerman, C. J., & Hinton, G. (2020). Backpropagation and the brain. *Nature Reviews Neuroscience*, *21*(6), Article 6. https://doi.org/10.1038/s41583-020-0277-3

Maia, T. V., & Frank, M. J. (2011). From reinforcement learning models to psychiatric and neurological disorders. *Nature Neuroscience*, *14*(2), Article 2. https://doi.org/10.1038/nn.2723

Mante, V., Sussillo, D., Shenoy, K. V., & Newsome, W. T. (2013). Context-dependent computation by recurrent dynamics in prefrontal cortex. *Nature*, *503*(7474), Article 7474. https://doi.org/10.1038/nature12742

Marcus, G. (2018). *Deep Learning: A Critical Appraisal* (arXiv:1801.00631). arXiv. https://doi.org/10.48550/arXiv.1801.00631

McClure, S., Gilzenrat, M. S., & Cohen, J. (2005, December 5). *An exploration-exploitation model based on norepinepherine and dopamine activity*. NIPS. https://www.semanticscholar.org/paper/An-exploration-exploitation-model-based-on-and-McClure-Gilzenrat/4ca689f5c8559b63268fdf12d2fbc56a24d2eb0f

Mei, J., Muller, E., & Ramaswamy, S. (2022). Informing deep neural networks by multiscale principles of neuromodulatory systems. *Trends in Neurosciences*, *45*(3), 237–250. https://doi.org/10.1016/j.tins.2021.12.008

Miller, K. J., Shenhav, A., & Ludvig, E. A. (2019). Habits without values. *Psychological Review*, *126*(2), 292–311. https://doi.org/10.1037/rev0000120

Mnih, V., Badia, A. P., Mirza, M., Graves, A., Harley, T., Lillicrap, T. P., Silver, D., & Kavukcuoglu, K. (2016). Asynchronous methods for deep reinforcement learning. *Proceedings of the 33rd International Conference on International Conference on Machine Learning - Volume 48*, 1928–1937.

Mnih, V., Kavukcuoglu, K., Silver, D., Rusu, A. A., Veness, J., Bellemare, M. G., Graves, A., Riedmiller, M., Fidjeland, A. K., Ostrovski, G., Petersen, S., Beattie, C., Sadik, A., Antonoglou, I., King, H., Kumaran, D., Wierstra, D., Legg, S., & Hassabis, D. (2015). Human-level control through deep reinforcement learning. *Nature*, *518*(7540), Article 7540. https://doi.org/10.1038/nature14236

Mohebi, A., Pettibone, J. R., Hamid, A. A., Wong, J.-M. T., Vinson, L. T., Patriarchi, T., Tian, L., Kennedy, R. T., & Berke, J. D. (2019). Dissociable dopamine dynamics for learning and motivation. *Nature*, *570*(7759), 65–70. https://doi.org/10.1038/s41586-019-1235-y

Munakata, Y., Morton, J. B., & Stedron, J. M. (2003). The role of prefrontal cortex in perseveration: Developmental and computational explorations. In *Connectionist models of development: Developmental processes in real and artificial neural networks* (pp. 83–114). Psychology Press.

O'Reilly, R. C., & Frank, M. J. (2006). Making working memory work: A computational model of learning in the prefrontal cortex and basal ganglia. *Neural Computation*, *18*(2), 283–328. https://doi.org/10.1162/089976606775093909

Parisotto, E., Song, F., Rae, J., Pascanu, R., Gulcehre, C., Jayakumar, S., Jaderberg, M., Kaufman, R. L., Clark, A., Noury, S., Botvinick, M., Heess, N., & Hadsell, R. (2020). Stabilizing Transformers for Reinforcement Learning. *Proceedings of the 37th International Conference on Machine Learning*, 7487–7498. https://proceedings.mlr.press/v119/parisotto20a.html

Platt, M. L., & Glimcher, P. W. (1999). Neural correlates of decision variables in parietal cortex. *Nature*, *400*(6741), Article 6741. https://doi.org/10.1038/22268

Pulvermüller, F., Tomasello, R., Henningsen-Schomers, M. R., & Wennekers, T. (2021). Biological constraints on neural network models of cognitive function. *Nature Reviews Neuroscience*, *22*(8), Article 8. https://doi.org/10.1038/s41583-021-00473-5

Qin, M., & Vucinic, D. (2018). *Training Recurrent Neural Networks against Noisy Computations during Inference* (arXiv:1807.06555). arXiv. https://doi.org/10.48550/arXiv.1807.06555

Rehmer, A., & Kroll, A. (2020). On the vanishing and exploding gradient problem in Gated Recurrent Units. *IFAC-PapersOnLine*, *53*(2), 1243–1248. https://doi.org/10.1016/j.ifacol.2020.12.1342

Renart, A., & Machens, C. K. (2014). Variability in neural activity and behavior. *Current Opinion in Neurobiology*, *25*, 211–220. https://doi.org/10.1016/j.conb.2014.02.013

Robertazzi, F., Vissani, M., Schillaci, G., & Falotico, E. (2022). Brain-inspired meta-reinforcement learning cognitive control in conflictual inhibition decision-making task

for artificial agents. *Neural Networks*, *154*, 283–302. https://doi.org/10.1016/j.neunet.2022.06.020

Roesch, M. R., & Olson, C. R. (2003). Impact of expected reward on neuronal activity in prefrontal cortex, frontal and supplementary eye fields and premotor cortex. *Journal of Neurophysiology*, *90*(3), 1766–1789. https://doi.org/10.1152/jn.00019.2003

Roesch, M. R., & Olson, C. R. (2007). Neuronal activity related to anticipated reward in frontal cortex: Does it represent value or reflect motivation? *Annals of the New York Academy of Sciences*, *1121*, 431–446. https://doi.org/10.1196/annals.1401.004

Schulz, E., & Gershman, S. J. (2019). The algorithmic architecture of exploration in the human brain. *Current Opinion in Neurobiology*, *55*, 7–14. https://doi.org/10.1016/j.conb.2018.11.003

Schulz, E., Wu, C. M., Ruggeri, A., & Meder, B. (2019). Searching for Rewards Like a Child Means Less Generalization and More Directed Exploration. *Psychological Science*, *30*(11), 1561–1572. https://doi.org/10.1177/0956797619863663

Silver, D., Hubert, T., Schrittwieser, J., Antonoglou, I., Lai, M., Guez, A., Lanctot, M., Sifre, L., Kumaran, D., Graepel, T., Lillicrap, T., Simonyan, K., & Hassabis, D. (2018). A general reinforcement learning algorithm that masters chess, shogi, and Go through self-play. *Science*, *362*(6419), 1140–1144. https://doi.org/10.1126/science.aar6404

Silver, D., Schrittwieser, J., Simonyan, K., Antonoglou, I., Huang, A., Guez, A., Hubert, T., Baker, L., Lai, M., Bolton, A., Chen, Y., Lillicrap, T., Hui, F., Sifre, L., van den Driessche, G., Graepel, T., & Hassabis, D. (2017). Mastering the game of Go without human knowledge. *Nature*, *550*(7676), Article 7676. https://doi.org/10.1038/nature24270

Song, H. F., Yang, G. R., & Wang, X.-J. (2017). Reward-based training of recurrent neural networks for cognitive and value-based tasks. *ELife*, *6*, e21492. https://doi.org/10.7554/eLife.21492

Speekenbrink, M., & Konstantinidis, E. (2015). Uncertainty and exploration in a restless bandit problem. *Topics in Cognitive Science*, *7*(2), 351–367. https://doi.org/10.1111/tops.12145

Stan Development Team. (2022). *RStan: The R interface to Stan*. http://mc-stan.org/

Sugrue, L. P., Corrado, G. S., & Newsome, W. T. (2004). Matching behavior and the representation of value in the parietal cortex. *Science (New York, N.Y.)*, *304*(5678), 1782–1787. https://doi.org/10.1126/science.1094765

Sussillo, D., & Barak, O. (2013). Opening the black box: Low-dimensional dynamics in high-dimensional recurrent neural networks. *Neural Computation*, *25*(3), 626–649. https://doi.org/10.1162/NECO_a_00409

Sutton, R. S., & Barto, A. G. (2018). *Reinforcement learning: An introduction* (Second edition). The MIT Press.

Swanson, K., Averbeck, B. B., & Laubach, M. (2020). *Noradrenergic regulation of Win-Stay/Lose-Shift policy and choice determinism in a two-armed bandit task* (p. 2020.11.13.382069). bioRxiv. https://doi.org/10.1101/2020.11.13.382069

Thorndike, E. L. (1927). The Law of Effect. *The American Journal of Psychology*, *39*(1/4), 212–222. https://doi.org/10.2307/1415413

Tsividis, P. A., Loula, J., Burga, J., Foss, N., Campero, A., Pouncy, T., Gershman, S. J., & Tenenbaum, J. B. (2021). *Human-Level Reinforcement Learning through Theory-Based Modeling, Exploration, and Planning* (arXiv:2107.12544). arXiv. http://arxiv.org/abs/2107.12544

Tsuda, B., Tye, K. M., Siegelmann, H. T., & Sejnowski, T. J. (2020). A modeling framework for adaptive lifelong learning with transfer and savings through gating in the prefrontal cortex. *Proceedings of the National Academy of Sciences*, *117*(47), 29872–29882. https://doi.org/10.1073/pnas.2009591117

Upadhyay, U., Shah, N., Ravikanti, S., & Medhe, M. (2019). *Transformer Based Reinforcement Learning For Games* (arXiv:1912.03918). arXiv. https://doi.org/10.48550/arXiv.1912.03918

Vehtari, A., Gabry, J., Magnusson, M., Yao, Y., Bürkner, P.-C., Paananen, T., & Gelman, A. (2022). *loo: Efficient leave-one-out cross-validation and WAIC for Bayesian models*. https://mc-stan.org/loo/

Vehtari, A., Gelman, A., & Gabry, J. (2017). Practical Bayesian model evaluation using leave-one-out cross-validation and WAIC. *Statistics and Computing*, *27*(5), 1413–1432. https://doi.org/10.1007/s11222-016-9696-4

Wang, J. X., Kurth-Nelson, Z., Kumaran, D., Tirumala, D., Soyer, H., Leibo, J. Z., Hassabis, D., & Botvinick, M. (2018). Prefrontal cortex as a meta-reinforcement learning system. *Nature Neuroscience*, *21*(6), Article 6. https://doi.org/10.1038/s41593-018-0147-8

Wauthier, S. T., Mazzaglia, P., Çatal, O., De Boom, C., Verbelen, T., & Dhoedt, B. (2021). *A learning gap between neuroscience and reinforcement learning* (arXiv:2104.10995). arXiv. https://doi.org/10.48550/arXiv.2104.10995

Wicherts, J. M., Veldkamp, C. L. S., Augusteijn, H. E. M., Bakker, M., van Aert, R. C. M., & van Assen, M. A. L. M. (2016). Degrees of Freedom in Planning, Running, Analyzing, and Reporting Psychological Studies: A Checklist to Avoid p-Hacking. *Frontiers in Psychology*, *7*, 1832. https://doi.org/10.3389/fpsyg.2016.01832

Wiehler, A., Chakroun, K., & Peters, J. (2021). Attenuated directed exploration during reinforcement learning in gambling disorder. *Journal of Neuroscience*. https://doi.org/10.1523/JNEUROSCI.1607-20.2021

Williams, R. J., & Peng, J. (1991). Function Optimization using Connectionist Reinforcement Learning Algorithms. *Connection Science*, *3*(3), 241–268. https://doi.org/10.1080/09540099108946587

Wilson, R. C., Bonawitz, E., Costa, V. D., & Ebitz, R. B. (2021). Balancing exploration and exploitation with information and randomization. *Current Opinion in Behavioral Sciences*, *38*, 49–56. https://doi.org/10.1016/j.cobeha.2020.10.001

Wilson, R. C., Geana, A., White, J. M., Ludvig, E. A., & Cohen, J. D. (2014). Humans Use Directed and Random Exploration to Solve the Explore–Exploit Dilemma. *Journal of*

Experimental Psychology. General, *143*(6), 2074–2081. https://doi.org/10.1037/a0038199

Worthy, D. A., Hawthorne, M. J., & Otto, A. R. (2013). Heterogeneity of strategy use in the Iowa gambling task: A comparison of win-stay/lose-shift and reinforcement learning models. *Psychonomic Bulletin & Review*, *20*(2), 364–371. https://doi.org/10.3758/s13423-012-0324-9

Wu, C. M., Schulz, E., Speekenbrink, M., Nelson, J. D., & Meder, B. (2018). Generalization guides human exploration in vast decision spaces. *Nature Human Behaviour*, *2*(12), Article 12. https://doi.org/10.1038/s41562-018-0467-4

Yahata, N., Kasai, K., & Kawato, M. (2017). Computational neuroscience approach to biomarkers and treatments for mental disorders. *Psychiatry and Clinical Neurosciences*, *71*(4), 215–237. https://doi.org/10.1111/pcn.12502

Zuhlsdorff, K. (2022). *Investigating reinforcement learning processes in depression and substance use disorder: Translational, computational and neuroimaging approaches.* [Thesis, Cambridge University]. https://doi.org/10.17863/CAM.91233

Supplement

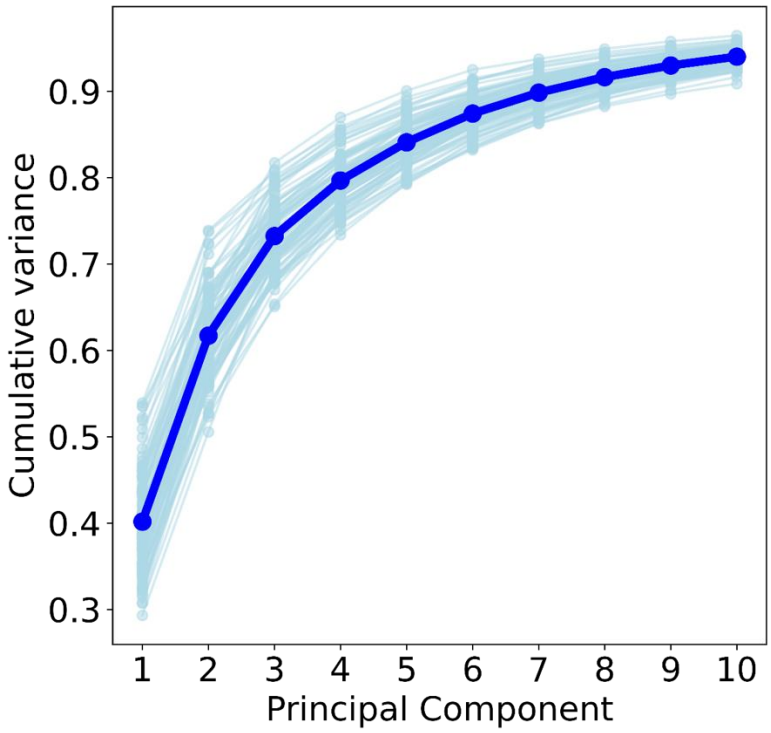

Supplemental Figure 1. Cumulative variance explained in hidden unit activity by principal components of the best RNN architecture (LSTM cell with weber noise, A2C algorithm and no entropy regularization): *Light blue lines denote cumulative variance explained for each RNN instance. Dark blue line denotes mean cumulative variance explained over all RNN instances.*

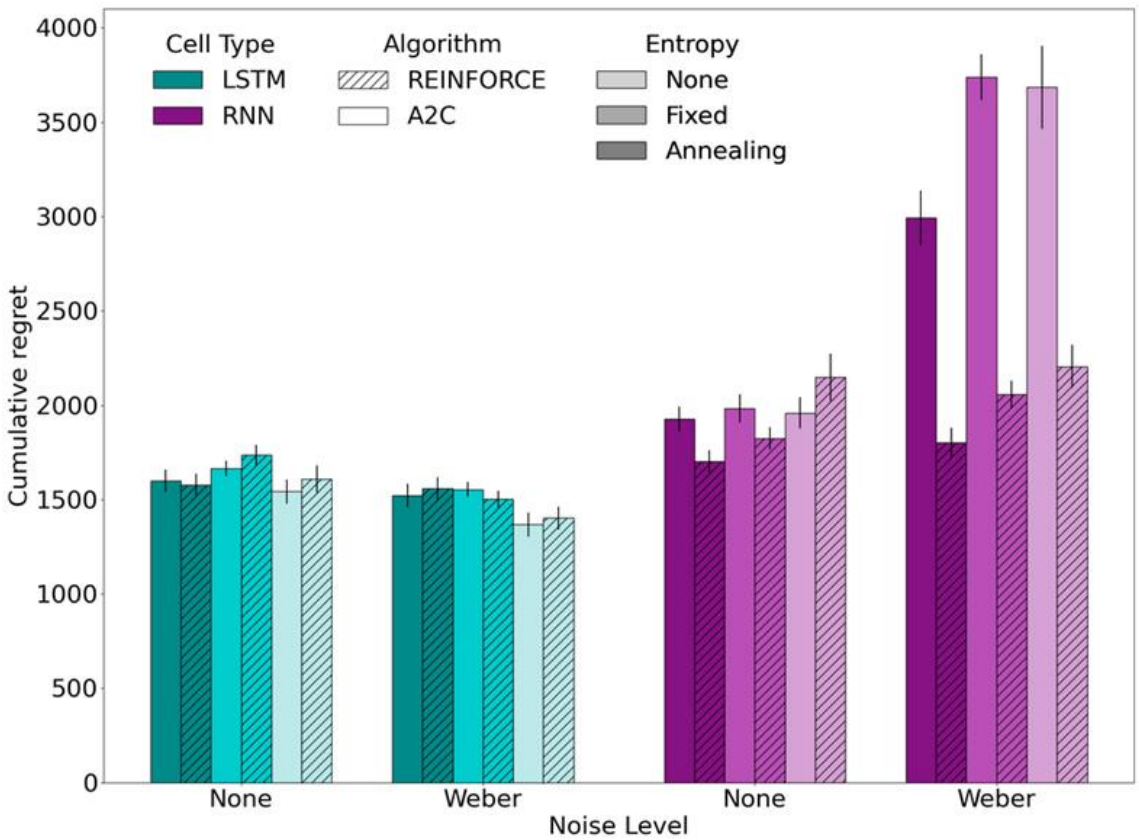

Supplemental Figure 2. Mean final cumulative regret of all rnn architectures in the restless bandit task by different design factors*. X-axis denote whether no computation noise ("None") or weber noise ("Weber") is added to hidden units. Error bars denote SEM.*

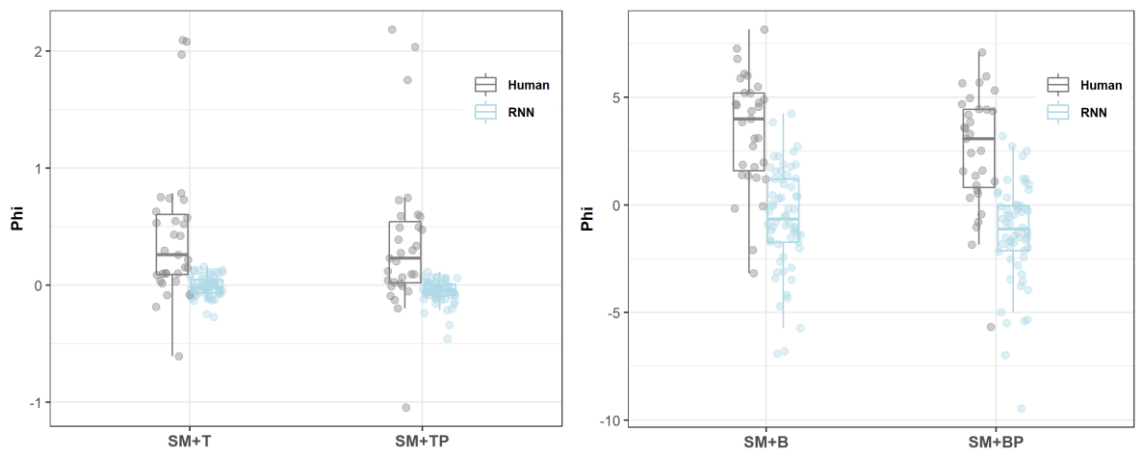

Supplemental Figure 3. Median exploration bonus parameter values (Phi) from the bayesian learner model for human subjects and RNN instances. *SM+T denotes a softmax decision rule with a trial-based directed exploration mechanism. SM + B denotes a softmax decision rule with a unique-bandit-based directed exploration mechanism. SM +TP and SM+BP denote respective models with an additive first-order perseveration term.*

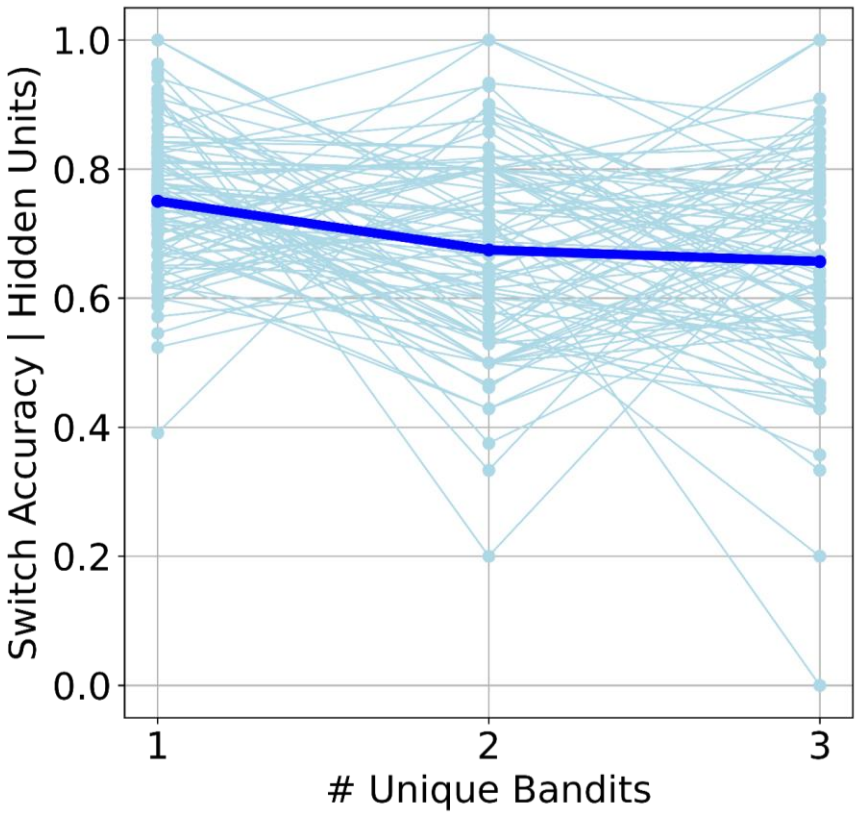

Supplemental Figure 4. *Switch accuracy given PCA-based de-noised hidden units of the RNN sorted by number of unique bandits sampled between consecutive switch trials (x-axis), where higher numbers reflect higher uncertainty. Solid lines indicate means and thin lines indicate individual instance data.*

Supplemental Table 1. *Model Comparison for the best performing RNN architecture (LSTM network with computational noise)*

Model	**Delta Rule**	**Bayesian Learner Rule**
SM	84.6 (54.7)	76.1 (41.9)
SM + E	-	21.3 (11.5)
SM + T	53.1 (20.5)	48.6 (19.2)
SM + B	22 (12.8)	19.7 (12)
SM + P	7.52 (6.75)	5.2 (7.87)
SM + EP	-	3.15 (4.04) *
SM + TP	7.57 (5.24)	4.73 (5.52)
SM + BP	7.64 (6.25)	6.22 (8.59)

Note: This table shows Delta WAIC values and standard deviations for each cognitive model in the model space (see Table 1) for the RNN data. The cognitive model with the lowest Delta WAIC value shows the best model fit.

Supplemental Table 2. *Model Comparison for human data*

Model	Delta Rule	Bayesian Learner Rule
SM	33.2 (21.7)	30.3 (18.8)
SM + E	-	20.2 (17.4)
SM + T	23.7 (20.1)	19.7 (15.1)
SM + B	26.7 (20.8)	23.8 (19.4)
SM + P	21.9 (18.4)	20.3 (17.9)
SM + EP	-	4.40 (5.01) *
SM + TP	9.82 (10.4)	7.70 (6.46)
SM + BP	11.6 (9.59)	9.84 (9.56)

Note: This table shows Delta WAIC values and standard deviations for each cognitive model in the model space (see Table 1) for human data. The cognitive model with the lowest Delta WAIC value shows the best model fit.

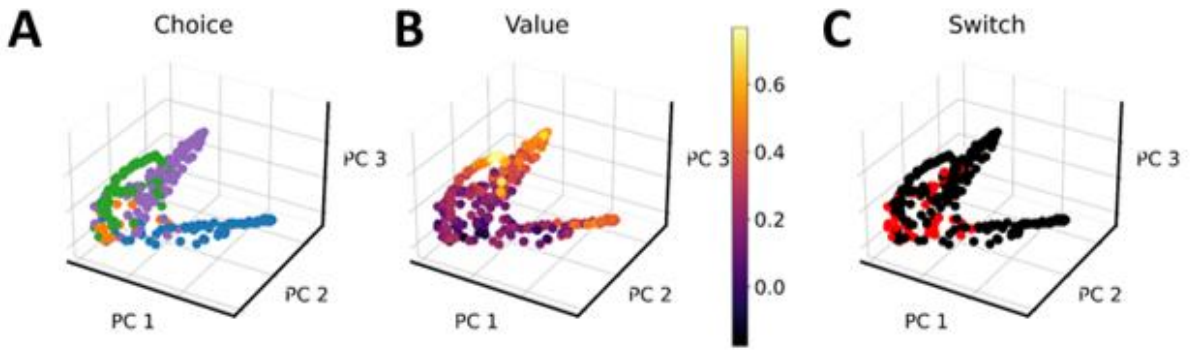

Supplemental Figure 5. *Hidden unit dynamics (first three principal components) of an example RNN agent color coded by choice (A), state-value estimate (B) and switching behavior (C, switch – red, stay - black). The pattern of choice-specific clusters (A), more overlap for actions corresponding to low state-value estimates (B) and switches occuring predominantly in this region of overlap (C) generalizes to all RNN instances under consideration (see below).*

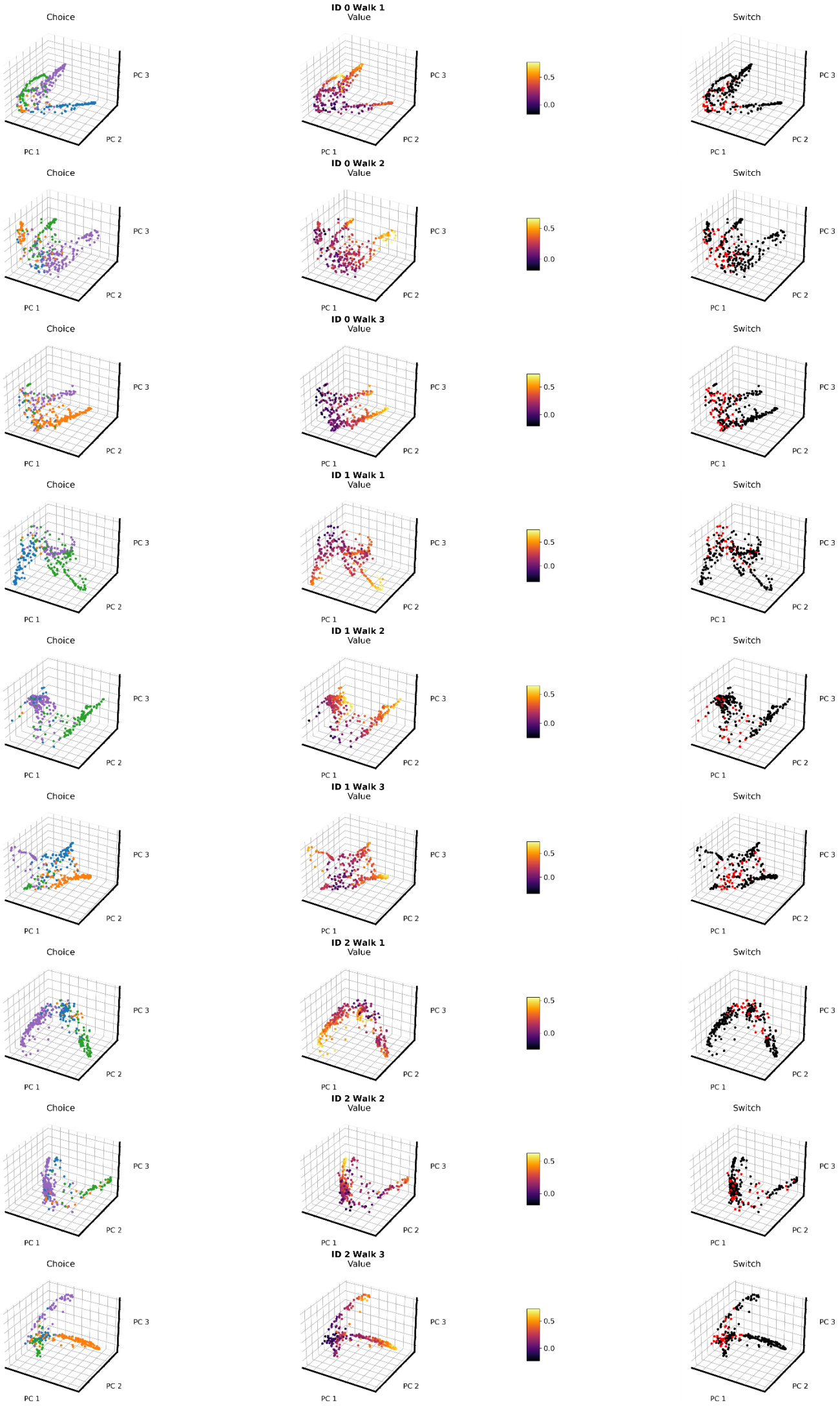
ID 0 Walk 1
Choice
Value
Switch
ID 0 Walk 2
Choice
Value
Switch
ID 0 Walk 3
Choice
Value
Switch
ID 1 Walk 1
Choice
Value
Switch
ID 1 Walk 2
Choice
Value
Switch
ID 1 Walk 3
Choice
Value
Switch
ID 2 Walk 1
Choice
Value
Switch
ID 2 Walk 2
Choice
Value
Switch
ID 2 Walk 3
Choice
Value
Switch
PC 1
PC 2
PC 3
0.5
0.0

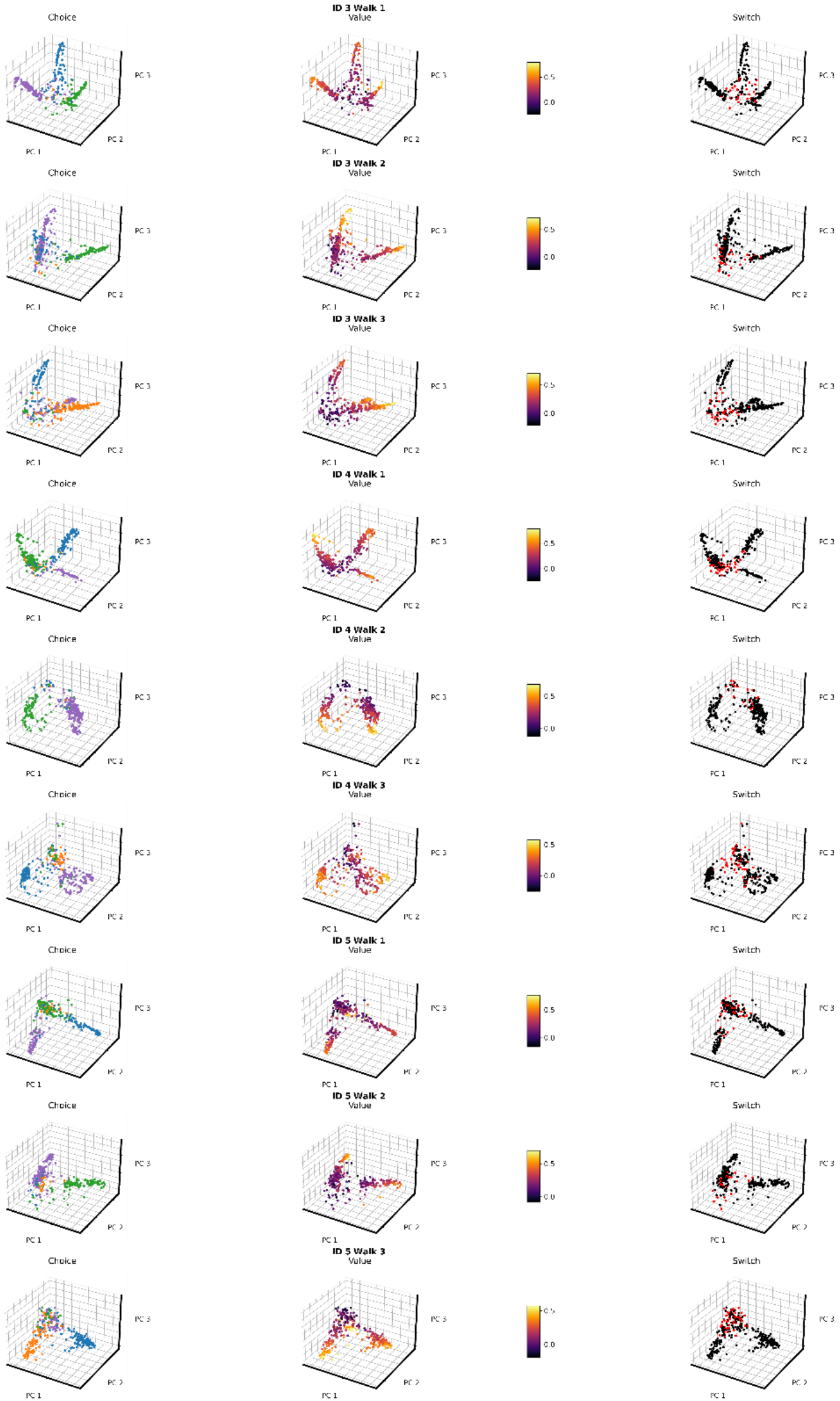
ID 3 Walk 1
Choice
Value
Switch
ID 3 Walk 2
Choice
Value
Switch
ID 3 Walk 3
Choice
Value
Switch
ID 4 Walk 1
Choice
Value
Switch
ID 4 Walk 2
Choice
Value
Switch
ID 4 Walk 3
Choice
Value
Switch
ID 5 Walk 1
Choice
Value
Switch
ID 5 Walk 2
Choice
Value
Switch
ID 5 Walk 3
Choice
Value
Switch
PC 1
PC 2
PC 3
0.5
0.0

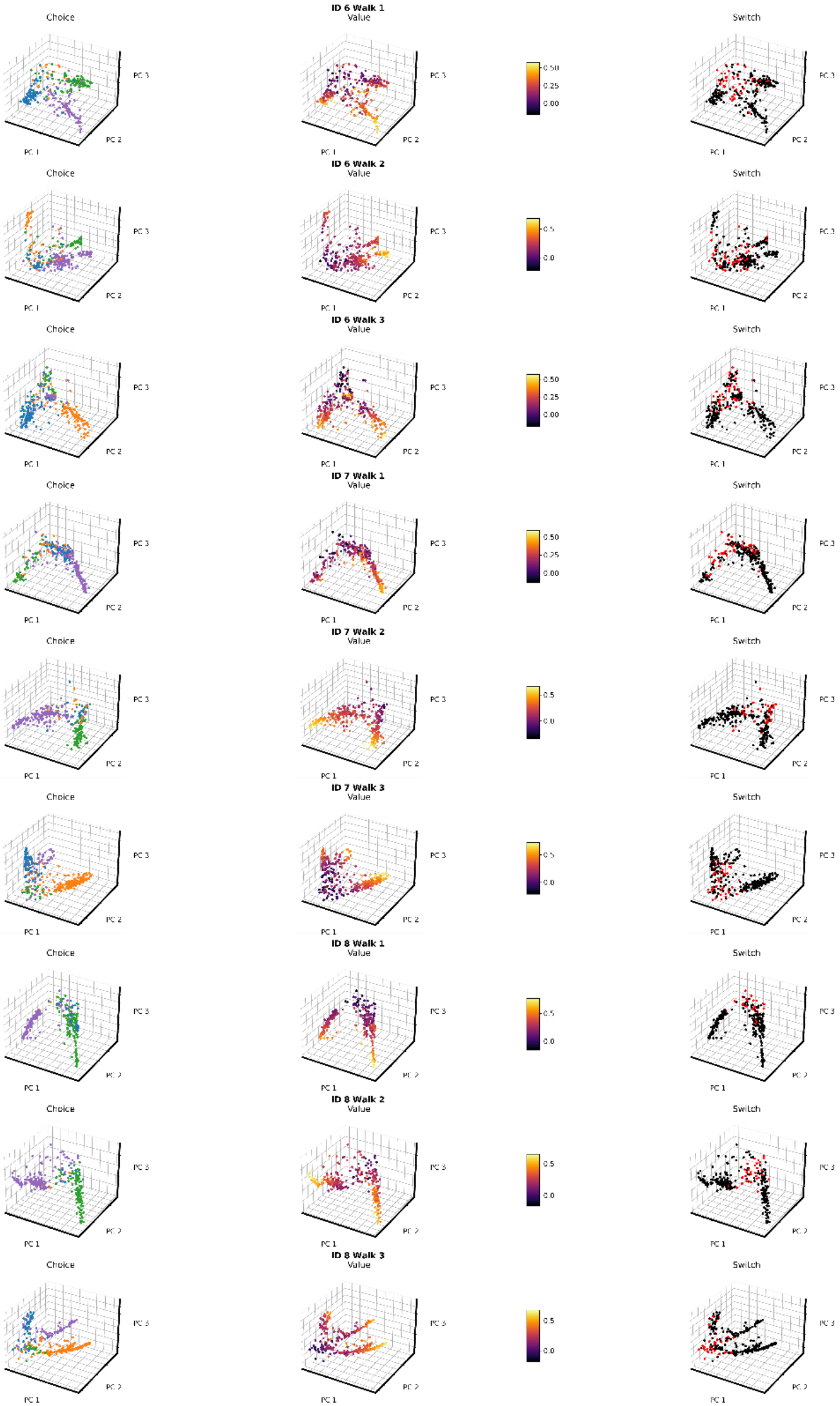
ID 6 Walk 1
Choice
Value
Switch
ID 6 Walk 2
Choice
Value
Switch
ID 6 Walk 3
Choice
Value
Switch
ID 7 Walk 1
Choice
Value
Switch
ID 7 Walk 2
Choice
Value
Switch
ID 7 Walk 3
Choice
Value
Switch
ID 8 Walk 1
Choice
Value
Switch
ID 8 Walk 2
Choice
Value
Switch
ID 8 Walk 3
Choice
Value
Switch
PC 1
PC 2
PC 3
0.50
0.25
0.00
0.5
0.0

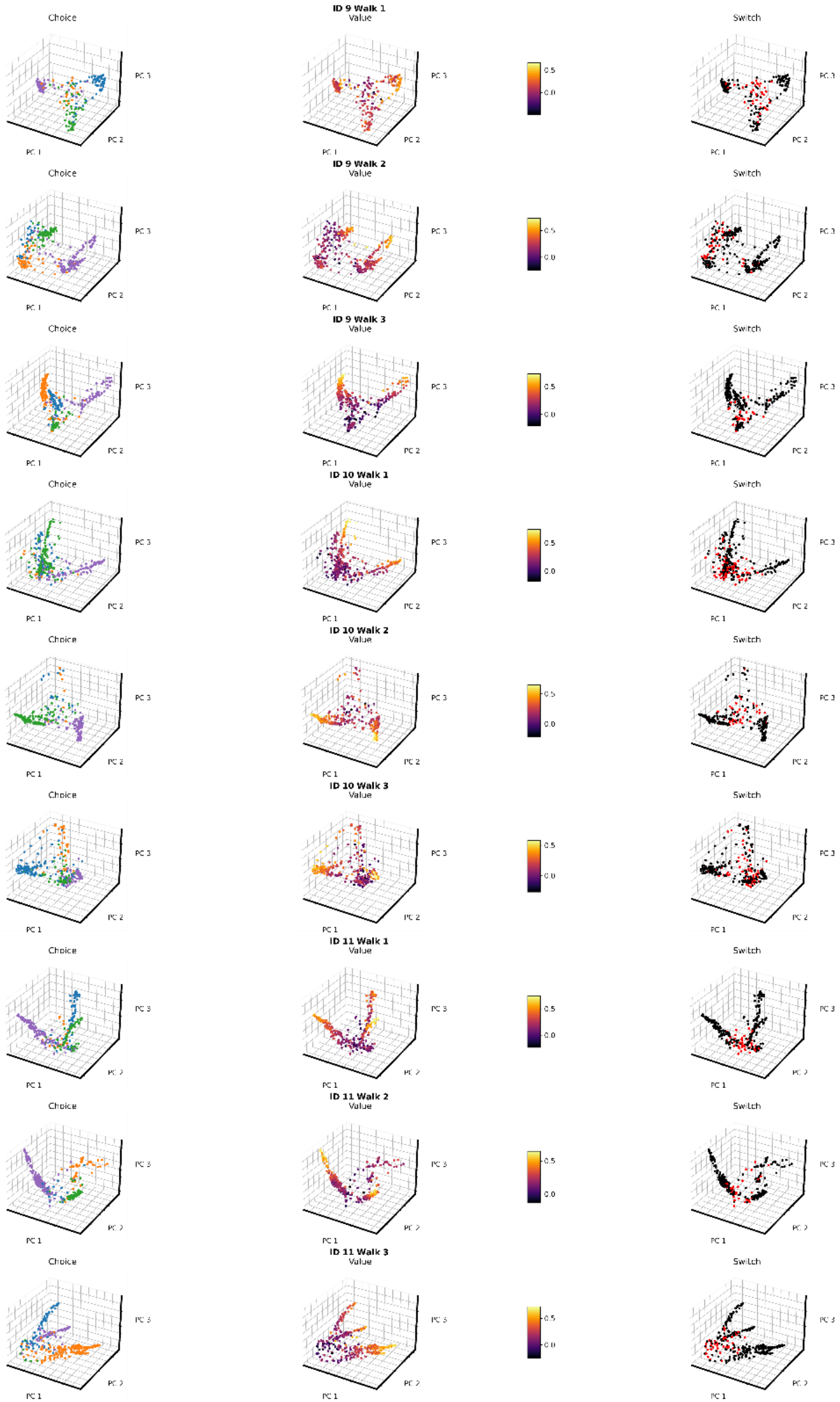
ID 9 Walk 1
Choice
Value
Switch
ID 9 Walk 2
Choice
Value
Switch
ID 9 Walk 3
Choice
Value
Switch
ID 10 Walk 1
Choice
Value
Switch
ID 10 Walk 2
Choice
Value
Switch
ID 10 Walk 3
Choice
Value
Switch
ID 11 Walk 1
Choice
Value
Switch
ID 11 Walk 2
Choice
Value
Switch
ID 11 Walk 3
Choice
Value
Switch
PC 1
PC 2
PC 3
0.5
0.0

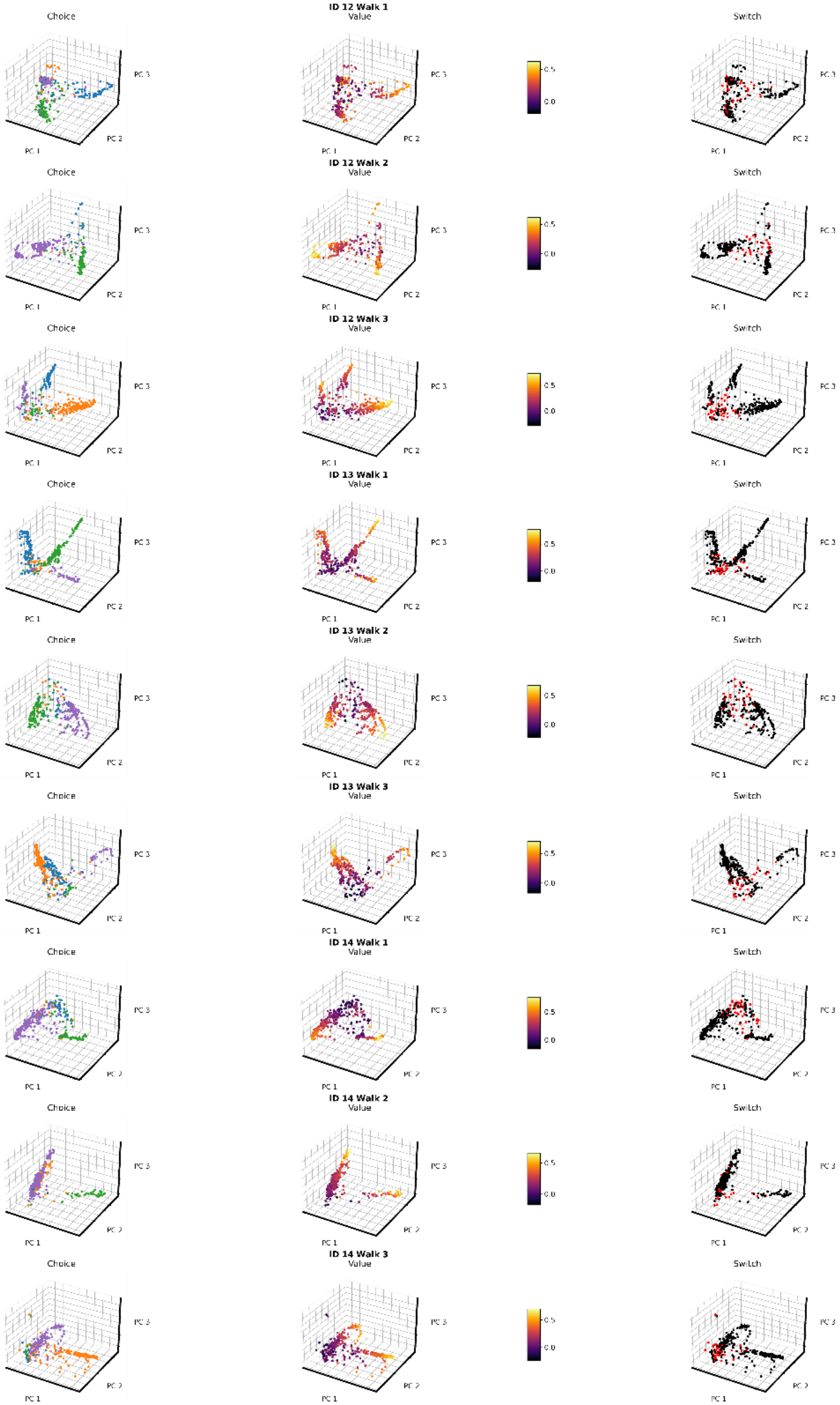
ID 12 Walk 1
Choice
Value
Switch
ID 12 Walk 2
Choice
Value
Switch
ID 12 Walk 3
Choice
Value
Switch
ID 13 Walk 1
Choice
Value
Switch
ID 13 Walk 2
Choice
Value
Switch
ID 13 Walk 3
Choice
Value
Switch
ID 14 Walk 1
Choice
Value
Switch
ID 14 Walk 2
Choice
Value
Switch
ID 14 Walk 3
Choice
Value
Switch
PC 1
PC 2
PC 3
0.5
0.0

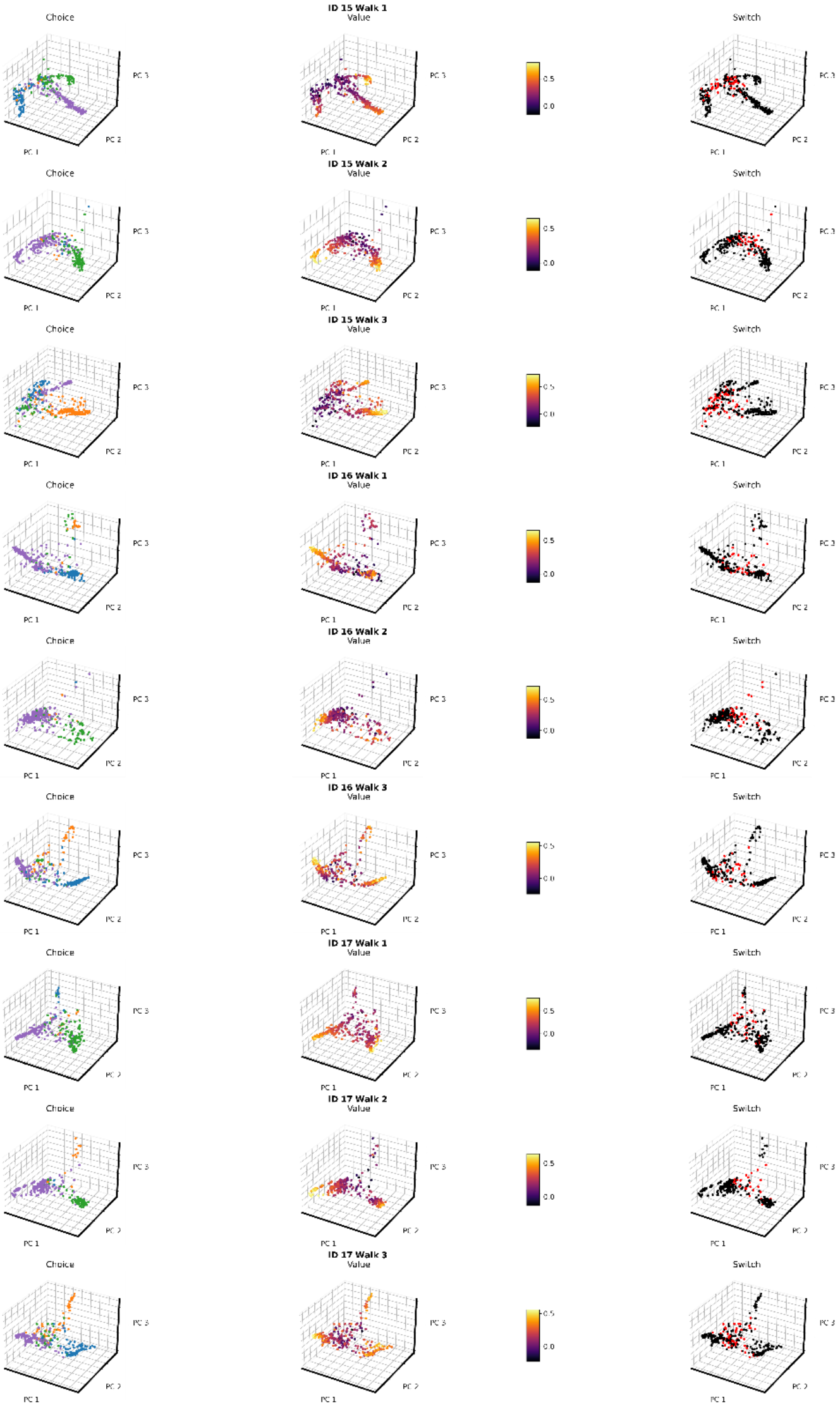
ID 15 Walk 1
Choice
Value
Switch
ID 15 Walk 2
Choice
Value
Switch
ID 15 Walk 3
Choice
Value
Switch
ID 16 Walk 1
Choice
Value
Switch
ID 16 Walk 2
Choice
Value
Switch
ID 16 Walk 3
Choice
Value
Switch
ID 17 Walk 1
Choice
Value
Switch
ID 17 Walk 2
Choice
Value
Switch
ID 17 Walk 3
Choice
Value
Switch
PC 1
PC 2
PC 3
0.5
0.0

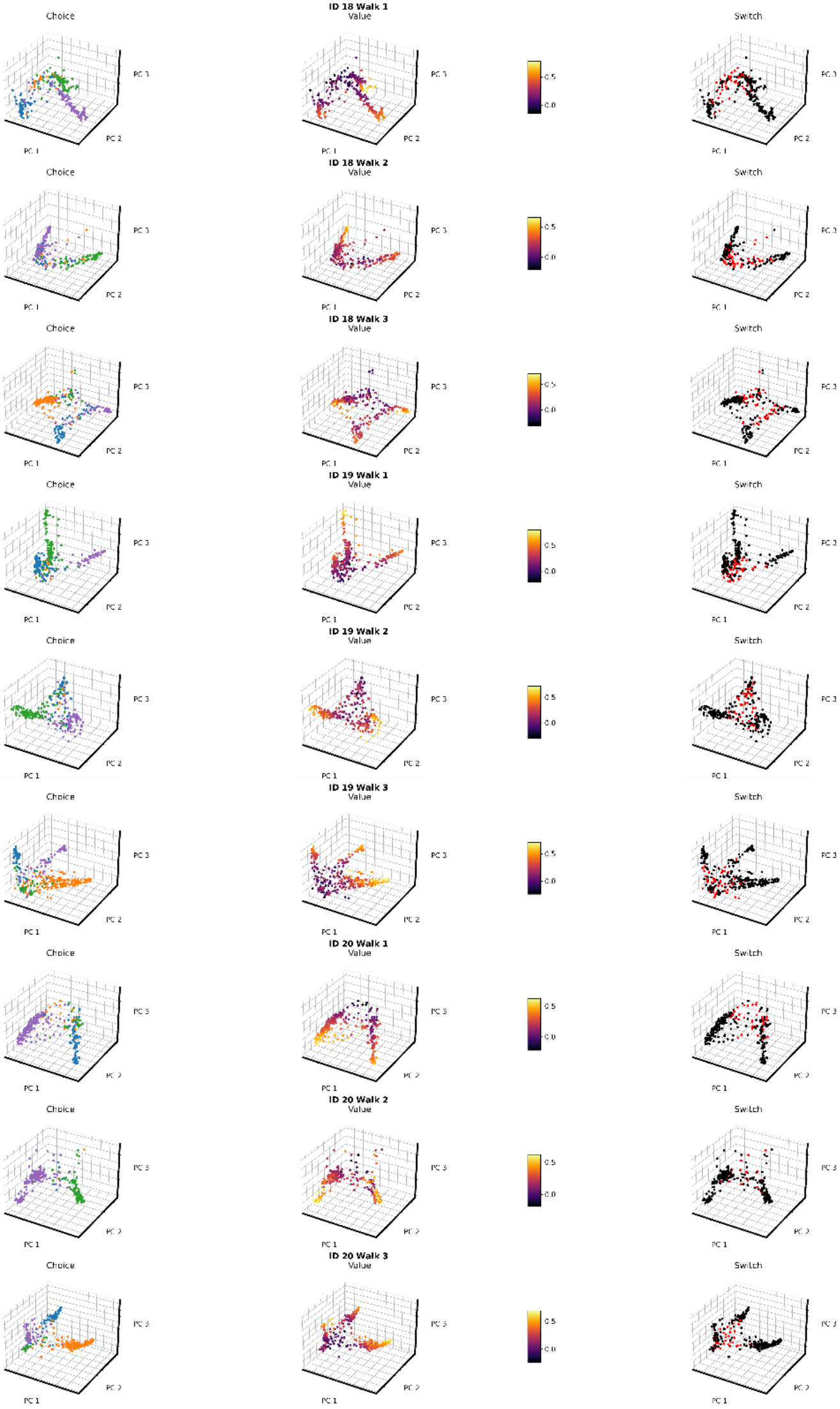
ID 18 Walk 1
Choice
Value
Switch
ID 18 Walk 2
Choice
Value
Switch
ID 18 Walk 3
Choice
Value
Switch
ID 19 Walk 1
Choice
Value
Switch
ID 19 Walk 2
Choice
Value
Switch
ID 19 Walk 3
Choice
Value
Switch
ID 20 Walk 1
Choice
Value
Switch
ID 20 Walk 2
Choice
Value
Switch
ID 20 Walk 3
Choice
Value
Switch
PC 1
PC 2
PC 3
0.5
0.0

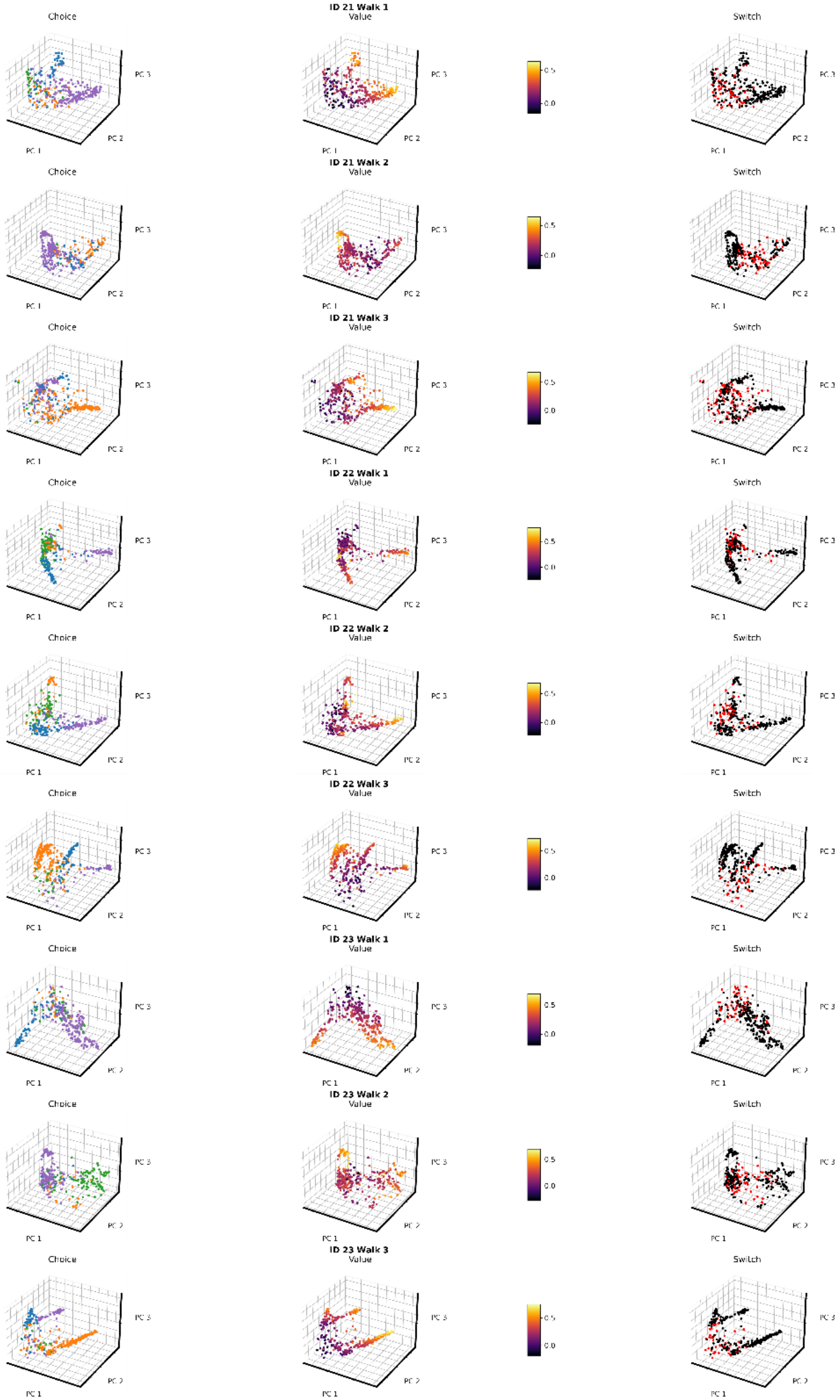
Choice
ID 21 Walk 1
Value
Switch
ID 21 Walk 2
ID 21 Walk 3
ID 22 Walk 1
ID 22 Walk 2
ID 22 Walk 3
ID 23 Walk 1
ID 23 Walk 2
ID 23 Walk 3
PC 1
PC 2
PC 3
0.5
0.0

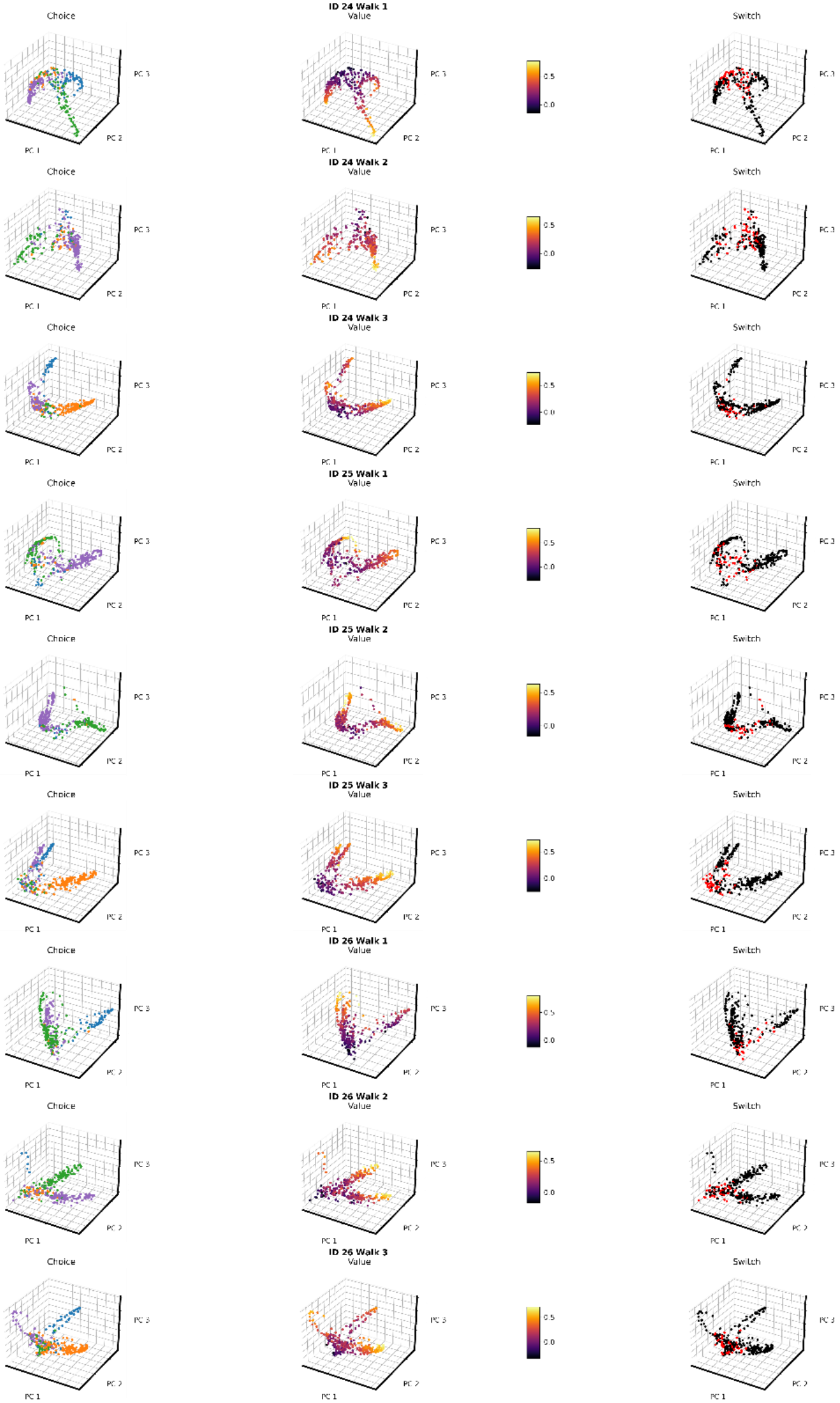
ID 24 Walk 1
Choice
Value
Switch
ID 24 Walk 2
Choice
Value
Switch
ID 24 Walk 3
Choice
Value
Switch
ID 25 Walk 1
Choice
Value
Switch
ID 25 Walk 2
Choice
Value
Switch
ID 25 Walk 3
Choice
Value
Switch
ID 26 Walk 1
Choice
Value
Switch
ID 26 Walk 2
Choice
Value
Switch
ID 26 Walk 3
Choice
Value
Switch
PC 1
PC 2
PC 3
0.5
0.0

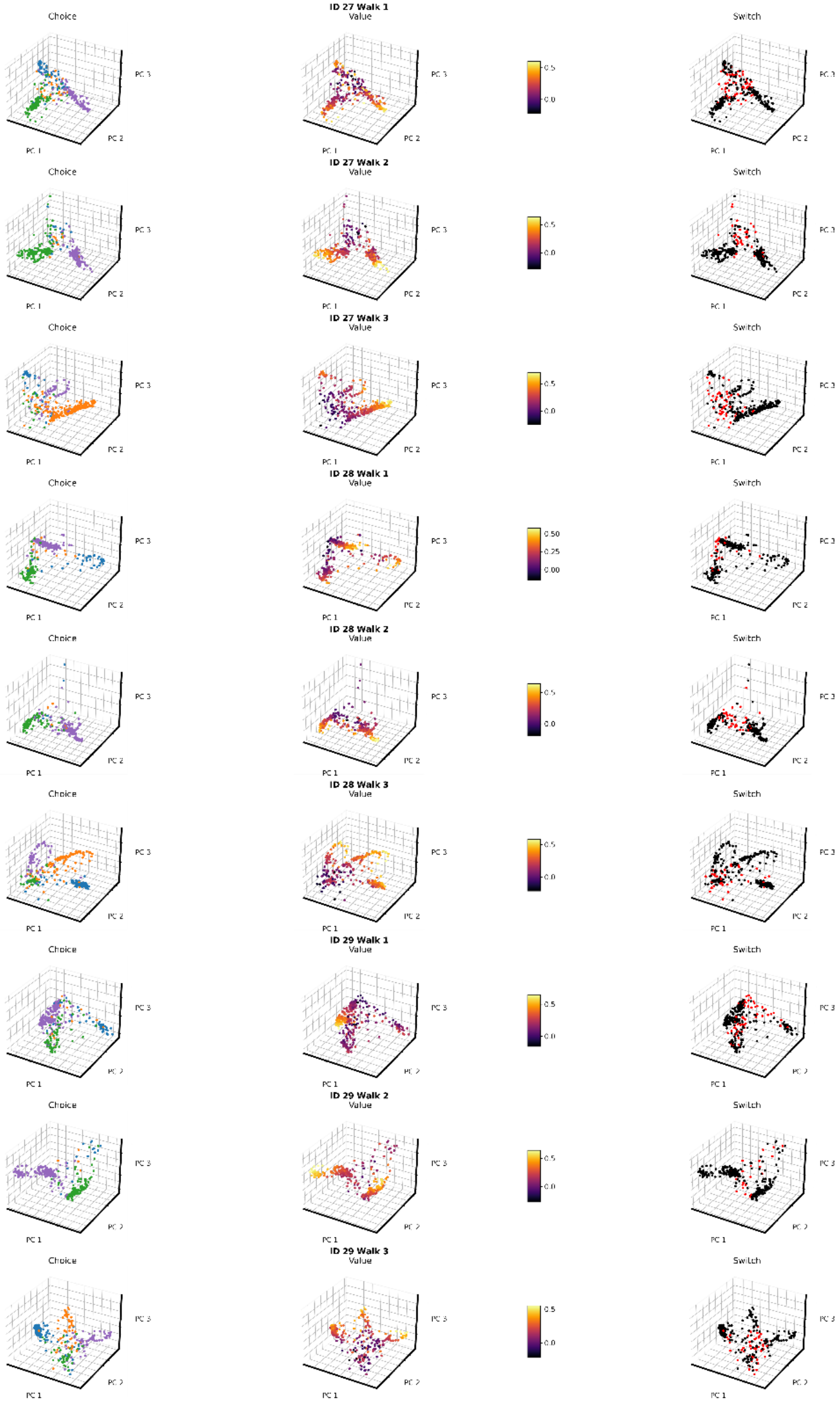
ID 27 Walk 1
Choice
Value
Switch
ID 27 Walk 2
Choice
Value
Switch
ID 27 Walk 3
Choice
Value
Switch
ID 28 Walk 1
Choice
Value
Switch
ID 28 Walk 2
Choice
Value
Switch
ID 28 Walk 3
Choice
Value
Switch
ID 29 Walk 1
Choice
Value
Switch
ID 29 Walk 2
Choice
Value
Switch
ID 29 Walk 3
Choice
Value
Switch
PC 1
PC 2
PC 3
0.5
0.0
0.50
0.25
0.00